OPEN ACCESS Freely available online

PLoS one

Novel, Objective, Multivariate Biomarkers Composed of Plasma Amino Acid Profiles for the Diagnosis and Assessment of Inflammatory Bowel Disease

Tadakazu Hisamatsu[1]*, Susumu Okamoto[1], Masaki Hashimoto[4], Takahiko Muramatsu[4], Ayatoshi Andou[4], Michihide Uo[4], Mina T. Kitazume[1], Katsuyoshi Matsuoka[1], Tomoharu Yajima[1], Nagamu Inoue[2], Takanori Kanai[1], Haruhiko Ogata[2], Yasushi Iwao[2], Minoru Yamakado[3], Ryosei Sakai[4], Nobukazu Ono[4], Toshihiko Ando[4], Manabu Suzuki[4], Toshifumi Hibi[1]*

1 Department of Internal Medicine, School of Medicine, Keio University, Tokyo, Japan, **2** Center for Diagnostic and Therapeutic Endoscopy, Keio University, Tokyo, Japan, **3** Center for Multiphasic Health Testing and Services, Mitsui Memorial Hospital, Tokyo, Japan, **4** Institute of Life Sciences and Pharmaceutical Research Laboratories, Ajinomoto Co. Inc., Kawasaki, Japan

Abstract

Background: Inflammatory bowel disease (IBD) is a chronic intestinal disorder that is associated with a limited number of clinical biomarkers. In order to facilitate the diagnosis of IBD and assess its disease activity, we investigated the potential of novel multivariate indexes using statistical modeling of plasma amino acid concentrations (aminogram).

Methodology and Principal Findings: We measured fasting plasma aminograms in 387 IBD patients (Crohn's disease (CD), n = 165; ulcerative colitis (UC), n = 222) and 210 healthy controls. Based on Fisher linear classifiers, multivariate indexes were developed from the aminogram in discovery samples (CD, n = 102; UC, n = 102; age and sex-matched healthy controls, n = 102) and internally validated. The indexes were used to discriminate between CD or UC patients and healthy controls, as well as between patients with active disease and those in remission. We assessed index performances using the area under the curve of the receiver operating characteristic (ROC AUC). We observed significant alterations to the plasma aminogram, including histidine and tryptophan. The multivariate indexes established from plasma aminograms were able to distinguish CD or UC patients from healthy controls with ROC AUCs of 0.940 (95% confidence interval (CI): 0.898–0.983) and 0.894 (95%CI: 0.853–0.935), respectively in validation samples (CD, n = 63; UC, n = 120; healthy controls, n = 108). In addition, other indexes appeared to be a measure of disease activity. These indexes distinguished active CD or UC patients from each remission patients with ROC AUCs of 0.894 (95%CI: 0.853–0.935) and 0.849 (95%CI: 0.770–0.928), and correlated with clinical disease activity indexes for CD ($r_s = 0.592$, 95%CI: 0.385–0.742, $p<0.001$) or UC ($r_s = 0.598$, 95%CI: 0.452–0.713, $p<0.001$), respectively.

Conclusions and Significance: In this study, we demonstrated that established multivariate indexes composed of plasma amino acid profiles can serve as novel, non-invasive, objective biomarkers for the diagnosis and monitoring of IBD, providing us with new insights into the pathophysiology of the disease.

Citation: Hisamatsu T, Okamoto S, Hashimoto M, Muramatsu T, Andou A, et al. (2012) Novel, Objective, Multivariate Biomarkers Composed of Plasma Amino Acid Profiles for the Diagnosis and Assessment of Inflammatory Bowel Disease. PLoS ONE 7(1): e31131. doi:10.1371/journal.pone.0031131

Editor: Jan-Hendrik Niess, Ulm University, Germany

Received September 9, 2011; **Accepted** January 3, 2012; **Published** January 31, 2012

Funding: This study was supported by grants-in-aid and "Academic Frontier" Project from the Japanese Ministry of Education, Culture and Science, the Japanese Ministry of Health, Labor and Welfare, Keio University and Keio Medical Foundation, Tokyo, Japan. The funders had no role in study design, data collection and analysis, decision to publish, or preparation of the manuscript. No additional external funding received for this study.

Competing Interests: MH, TM, AA, MU, RS, NO, TA, and MS are employees of Ajinomoto, Co., Inc. T.Hisamatsu, SO, KM, TY, NI, TK, HO, YI, and T.Hibi received research grants from Ajinomoto, Co., Inc. TM, AA, T.Hibi, T.Hisamatsu, SO, RS, NO, MS, TA and MH have applied for patents for plasma amino-acid profiling using multivariate analysis as a diagnostic tool for IBD (WO2008/090941). This does not alter the authors' adherence to all the PLoS One policies on sharing data and materials.

* E-mail: thibi@sc.itc.keio.ac.jp (T.Hibi); hisamachi@a7.keio.jp (T.Hisamatsu)

Introduction

Inflammatory bowel disease (IBD) is a chronic intestinal disorder comprising two major types, Crohn's disease (CD) and ulcerative colitis (UC) [1,2]. Despite intensive research, the etiology of IBD remains unknown, although it is considered to be a multi-factorial disease determined by genetic backgrounds, environmental factors and immunological disorders.

Importantly, the number of patients with IBD and colorectal cancers in Asia has increased remarkably during the past decade. One of the reasons for this change is thought to be the move towards a more Westernized diet. Dietary habits are recognized to be an important modifiable environmental factor influencing the risk of these diseases. Most physicians believe in the role of diet and nutritional metabolism in IBD pathogenesis, however, clinical and basic research has not adequately addressed these issues.

The human body is a highly organized metabolic network of systems that regulates individual homeostasis, but it is often difficult to objectively assess. Analysis of the metabolomic condition instead is therefore of use in determining health status, as disturbances of metabolic homeostasis are known to be related to the pathogenesis of metabolic syndromes, chronic inflammatory disorders, and cancers. Post-genomic technologies, in particular metabolomics, provide new opportunities to study metabolic effects in relation to disease. Metabolomics is a rapidly evolving field that comprehensively measures metabolites, ideally in a biological fluid, and changes in metabolic profiles are a potential source of biomarkers.

Overall, 20% of the human body is composed of amino acids (AAs) and their metabolites, which play important roles as both basic substrates and regulators in many metabolic pathways [3,4]. Specific abnormalities in plasma AA concentrations have been reported in the context of various diseases, such as Fischer's ratio in fibrotic liver disease [5,6,7,8]. Plasma AA profiling is also a potential screening tool for non-small cell lung carcinoma (NSCLC) [9].

Previously, we demonstrated that aminograms and the generation of a multivariate index using "AminoIndex™ technology" (MIAI) have the potential for diagnostic use, disease activity monitoring, and the assessment of pathophysiological conditions [10]. Here, we introduced the concept of metabolomics to analyse AA metabolism in IBD patients, and found that AA metabolism was disturbed in IBD patients, particularly those with active disease. AA profiles may reflect the nutritional condition of individuals, disease activity, and differences in pathogenesis between CD and UC. Finally, we established the novel clinical parameter, the MIAI which discriminated between CD and UC, and also reflected disease activity. We demonstrate for the first time that disturbances of AA metabolism are related to the pathophysiological state of IBD and that the MIAI is a novel, non-invasive, diagnostic and monitoring marker for IBD.

Methods

Patients

IBD patients (n = 387) were recruited between February 27, 2005, and March 7, 2008, at the Keio University Hospital, Tokyo, Japan. Healthy controls (HCs; n = 210) were recruited between December 1, 2005, and April 1, 2006, from the Center for Multiphasic Health Testing and Services, Mitsui Memorial Hospital, Tokyo, Japan. Patients and HCs were divided into discovery and validation sets. For the discovery screening, plasma samples were obtained from CD patients (n = 102), UC patients (n = 102) and age and sex-matched HCs (n = 102). For the validation test, plasma samples were obtained from CD patients (n = 63), UC patients (n = 120) and HCs (n = 108).

Patient and HC characteristics are shown in Table 1. For continuous monitoring, IBD patients (n = 22) were recruited between May 30, 2005, and February 18, 2010, at Keio University Hospital. This study was conducted in accordance with the Declaration of Helsinki, and the protocol was approved by the ethics committees of the Keio University School of Medicine and the Mitsui Memorial Hospital. Signed informed consent forms were obtained from all patients and all data were analyzed anonymously throughout the study. The diagnosis of UC and CD was based on established clinical, radiographic, endoscopic, and histopathologic criteria. Patient characteristics were determined from medical records, questionnaires, and interviews. Disease activity was assessed by the Crohn's disease activity index (CDAI) [11] and the *Lichtiger* Clinical Activity Index (CAI) [12]. Active disease was defined as CDAI≥150 for patients with CD and CAI≥5 for patients with UC. Remission was defined as CDAI<150 for patients with CD and CAI<5 for patients with UC.

Plasma AA analysis

Plasma samples for AA analysis were obtained using EDTA as an anticoagulant and stored at −80°C until analysis. Frozen plasma samples were briefly thawed, mixed with 5-sulfosalicylic acid (final concentration, 2.3%), then centrifuged for 10 min at 11,000× *g* at 4°C to remove precipitated proteins. Measurement of AA concentrations was performed using an automatic AA analyzer (L-8500; Hitachi High-Technologies Corporation, Tokyo, Japan). Briefly, AAs separated by cation-exchange chromatography were detected spectrophotometrically after a post-column reaction with ninhydrin reagent. We confirmed that the fasting plasma aminograms remained constant for individuals in this protocol.

Statistical analysis

For comparisons between study groups, we used the Mann-Whitney U test with Bonferroni correction. The Spearman correlation was used to test associations of CDAI, CAI and serum C-reactive protein (CRP) with the MIAI. These univariate statistical analyses were performed using Prism software, version 5.0.1 (Graph Pad Software, San Diego, CA). Correlation scatterplot analyses were carried out using JMP software, version 6.0.3 (SAS Institute Inc., Cary, NC). Multiple discriminant analyses were performed in the discovery set, then validated in the validation set with MATLAB software, version 7.6.0 (Mathworks, Natick, MA). Model performances were assessed using the area under the ROC curve (ROC AUC) as a measure of the validity of the MIAI. Details are given in Methods S1.

Results

Plasma His and Trp concentrations in IBD patients

Analysis of serum protein levels showed that serum albumin, but not total protein level, was decreased in IBD patients. Interestingly, the concentrations of several plasma AAs (e.g. histidine (His) and tryptophan (Trp)) were significantly decreased, while the levels of others were maintained in IBD patients (Table 2). Therefore, the observed changes in the concentrations of plasma AAs suggested that there is a metabolic alteration that occurs in patients with IBD.

As shown in Figure 1A and Table 2, plasma His concentrations were significantly decreased in both CD and UC patients compared with HCs (mean plasma His concentrations, 72.3 μM in CD patients and 71.0 μM in UC patients vs. 83.3 μM in HCs, $p<0.001$). Furthermore, the plasma His concentration showed significant decreases in patients with active disease (Figure 1B). Specifically, the mean plasma His concentration was 62.0 μM in CD patients with active disease (CDa) compared with 74.6 μM in CD patients in remission (CDr) ($p<0.001$). Similarly, the plasma His concentration was 65.0 μM in UCa patients compared with 76.6 μM in UCr patients ($p<0.001$). The plasma His concentration showed an inverse correlation with the CDAI in CD patients (Spearman's rank correlation coefficient $r_s = -0.386$, $p<0.001$) and the CAI in UC patients ($r_s = -0.425$, $p<0.001$) (Figure 1C). Most importantly, the plasma His concentration showed a highly inverse correlation with serum CRP levels in CD patients ($r_s = -0.460$, $p<0.001$) (Figure 1D and Table 3). Plasma Trp concentrations were also significantly decreased in IBD patients and inversely correlated with disease activity and serum CRP level.

Table 1. Patient characteristics.

		CD	UC	HC
Discovery Set	N	102	102	102
	Age, years	36.1±9.9	35.9±9.4	36.4±8.6
	Female, n (%)	32 (31)	32 (31)	32 (31)
	Mean disease duration, years	11.0±7.4	7.8±6.7	–
	Mean age at diagnosis, years	25.1±7.7	28.1±8.5	–
	Active disease	29	38	–
	CD characteristics			
	Disease location			
	Small bowel	31	–	–
	Colon	9	–	–
	Both	59	–	–
	Others	3	–	–
	Behavior (Montreal classification)			
	B1: non-stricturing, non-penetrating	26	–	–
	B2: stricturing	42	–	–
	B3: penetrating	34	–	–
	p: perianal disease modifier	40	–	–
	UC characteristics			
	Disease location			
	Proctitis	–	12	–
	Left sided colitis	–	43	–
	Entire colitis	–	47	–
	Treatment			
	Enteral nutrition	44	1	–
	Steroids	12	37	–
	Salicylates	91	98	–
	Immunosuppressors	56	25	–
	Infliximab	14	0	–
	Biomarker levels	Median (interquartile range)		
	Albumin (mg/dl)	4.2 (3.8–4.4)	4.5 (4.1–4.6)	4.6 (4.4–4.8)
	C-reactive Protein (mg/dl)	0.22 (0.03–0.77)	0.19 (0.03–0.25)	0.02 (0.01–0.04)
	Hemoglobin (g/dl)	12.8 (11.5–13.9)	13.9 (13.3–14.8)	15.2 (13.6–15.7)
Validation Set	n	63	120	108
	Age, years	32.3±11.2	42.6±16.2	42.4±7.9
	Female, n (%)	20 (33)	40 (33)	34 (32)

Plus-minus values are means±standard deviation.
doi:10.1371/journal.pone.0031131.t001

Multivariate-correlation analysis reveals alteration of AA metabolism in IBD patients

To analyze AA metabolomics in IBD patients, we measured 22 fasting plasma AA concentrations, then carried out multivariate-correlation analyses of these in IBD patients (UC: blue; CD: red) and HCs (green) (Figure S1). The scatter plots for two plasma AAs showed various patterns, and we observed a general imbalance of branched-chain AAs (BCAAs) in IBD patients (Figure S2A, B).

MIAI for clinical diagnosis of IBD

Although we found that AA metabolism is altered in IBD patients, it is difficult to establish a biomarker for clinical use based on these measurements. To overcome this, we tried to assess the AA metabolic condition of individuals by multivariate discriminant analysis of the plasma aminogram in the discovery set. The MIAI established from the plasma aminograms discriminated CD and UC patients from HCs with high specificity and sensitivity in the discovery set: (Index (CD/HC) = 22.435+5.184×[Tau] −2.678×[His]−4.520×[Tyr]−8.165×[Val]+7.210×[Ile], ROC AUC = 0.955; Index (UC/HC) = 27.422−7.5988×[His]+4.621×[Tau]−2.107×[Tyr]−4.964×[Asn]+2.930×[Thr], ROC AUC = 0.912) (Figure 2A and Table S1). These were then validated in additional IBD patients (ROC AUC of 0.940 for Index (CD/HC) and of 0.894 for Index (UC/HC), respectively) (Figure 2A). Importantly, the AA components between Index (CD/HC) and Index (UC/HC) differed, suggesting that AA metabolism differs between the two diseases. Therefore, the MIAI may reflect not

Table 2. Comparison of plasma amino acid (AA) concentrations in healthy control subjects, Crohn's disease and ulcerative colitis patients.

	HC	CD	UC	p
Albumin (g/dl)	4.6±0.2	4.1±0.5[2]	4.3±0.5[2]	<0.001[1]
Total Protein (g/dl)	7.2±0.3	7.3±0.7	7.4±0.5[2]	<0.001[1]
EAA				
Valine	219 (190–241)	195 (161–216)[4]	191 (166–221)[4]	<0.001[3]
Leucine	118 (98–135)	102 (84–119)[4]	101 (85–117)[4]	<0.001[3]
Isoleucine	61 (49–68)	57 (51–65)	54 (44–63)[4]	0.028[3]
Threonine	121 (108–134)	117 (97–146)	110 (94–130)[4]	0.036[3]
Lysine	192 (172–208)	187 (163–206)	174 (148–197)[4]	0.005[3]
Methionine	27 (24–29)	25 (21–29)[4]	23 (20–26)[4]	<0.001[3]
Histidine	83 (77–89)	72 (66–79)[4]	72 (66–81)[4]	<0.001[3]
Tryptophan	49 (42–56)	45 (38–52)[4]	48 (40–55)	0.05[3]
Phenylalanine	58 (51–63)	52 (46–61)[4]	54 (47–58)[4]	<0.001[3]
NEAA				
Glutamic acid	32 (25–42)	39 (30–51)	39 (29–50)	<0.001[3]
Asparagine	46 (41–51)	41 (37–48)[4]	40 (35–46)[4]	<0.001[3]
Serine	114 (98–129)	107 (97–122)	110 (85–124)	0.137[3]
Glutamine	565 (525–613)	544 (494–592)	550 (474–590)[4]	0.019[3]
Glycine	231 (205–264)	241 (205–286)	218 (185–251)[4]	0.002[3]
Proline	122 (105–144)	145 (114–181)[4]	125 (102–166)	0.001[3]
Tyrosine	61 (55–68)	52 (44–60)[4]	53 (46–60)[4]	<0.001[3]
Arginine	91 (78–103)	89 (74–104)	87 (72–96)	0.254[3]
Alanine	319 (265–362)	322 (261–379)	308 (271–356)	0.887[3]
Other				
Citrulline	31 (26–35)	28 (23–35)	28 (23–32)[4]	0.003[3]
Taurine	49 (44–56)	73 (58–99)[4]	68 (53–86)[4]	<0.001[3]
Ornithine	57 (51–68)	57 (48–67)	50 (44–58)[4]	<0.001[3]
Sum of EAAs	932 (845–1019)	856 (761–963)[4]	830 (745–915)[4]	<0.001[3]
Sum of NEAAs	1615 (1490–1714)	1463 (1104–1713)[4]	1562 (1395–1688)	0.002[3]
EAA/NEAA	0.58 (0.54–0.63)	0.58 (0.52–0.71)	0.55 (0.50–0.58)[4]	<0.001[3]

Serum albumine and total protein concentration are presented as mean±standard deviation. Plasma amino acid concentrations are presented as median (interquartile range).
[1]One-way analysis of variance test.
[2]Significantly different from control subjects, p<0.01 (by Dunnett's test).
[3]Kruskal Wallis Test.
[4]Significantly different from control subjects, p<0.01 (by Kruskal-Wallis after adjustment for CD and UC vs. HC by Dunn's test).
doi:10.1371/journal.pone.0031131.t002

only the inflammatory condition, but also the disease-specific AA metabolism of IBD patients.

According to these observations, we hypothesized that the MIAI is also useful for discrimination between CD and UC patients. As shown in Figure 2B, the MIAI could discriminate between CDa and UCa patients (Index (CDa/UCa) = −15.134+5.251×[Ile]+2.618×[Thr]+2.634×[Tau]−5.125×[Trp]−2.485×[Ar], ROC AUC = 0.879). By contrast, the MIAI showed less sensitivity and specificity for discrimination between CDr and UCr patients (Index (CDr/UCr) = 8.097−2.443×[Tyr]+2.327×[Gly]−2.633×[Val]+3.267×[Ile]−2.174×[Ser], ROC AUC = 0.744) (Figure 2B). These results indicate that the differences in metabolic conditions between UC and CD are more defined in active diseases, suggesting that an MIAI based on plasma AA profiling has the potential for diagnostic use.

MIAI for assessing IBD disease activity

Next, we investigated the ability of the MIAI to assess disease activity. The MIAI could discriminate between patients with active disease and those in remission among both CD and UC patients (CDa vs. CDr: Index (CDa/CDr) = 16.474−3.342×[His]−5.190×[Trp]+1.857×[Tau]+2.715×[Met], ROC AUC = 0.894; UCa vs. UCr: Index (UCa/UCr) = 34.019−2.926×[Trp]−1.864×[Tyr]−4.777×[Val]−2.856×[Met]+4.604×[Ile], ROC AUC = 0.849) (Figure 3A). As shown in Figure 3B, Index (CDa/CDr) was unable to identify the activity of UC, indicating that this index specifically identified the activity of CD. Furthermore, Index (CDa/CDr) and Index (UCa/UCr) showed a positive correlation with the CDAI ($r_s = 0.592$, $p<0.001$) and CAI ($r_s = 0.598$, $p<0.001$), respectively (Figure 3C).

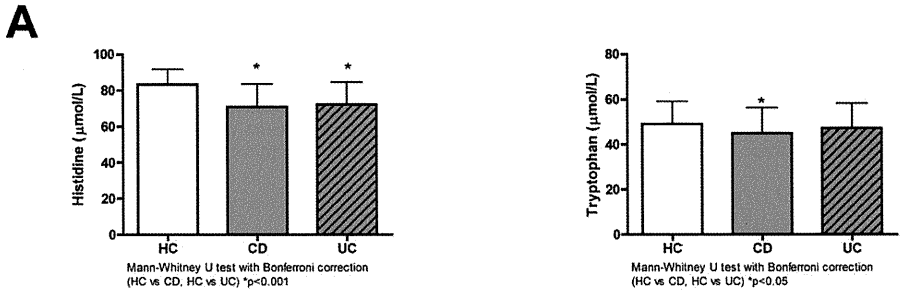
A
Histidine (µmol/L)
HC
CD
UC
Mann-Whitney U test with Bonferroni correction
(HC vs CD, HC vs UC) *p<0.001
Tryptophan (µmol/L)
HC
CD
UC
Mann-Whitney U test with Bonferroni correction
(HC vs CD, HC vs UC) *p<0.05

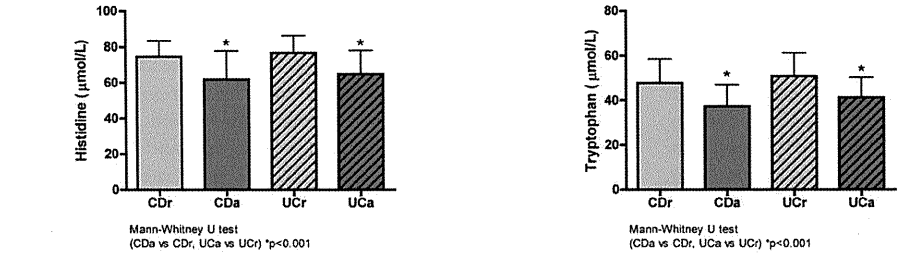
B
Histidine (µmol/L)
CDr
CDa
UCr
UCa
Mann-Whitney U test
(CDa vs CDr, UCa vs UCr) *p<0.001
Tryptophan (µmol/L)
CDr
CDa
UCr
UCa
Mann-Whitney U test
(CDa vs CDr, UCa vs UCr) *p<0.001

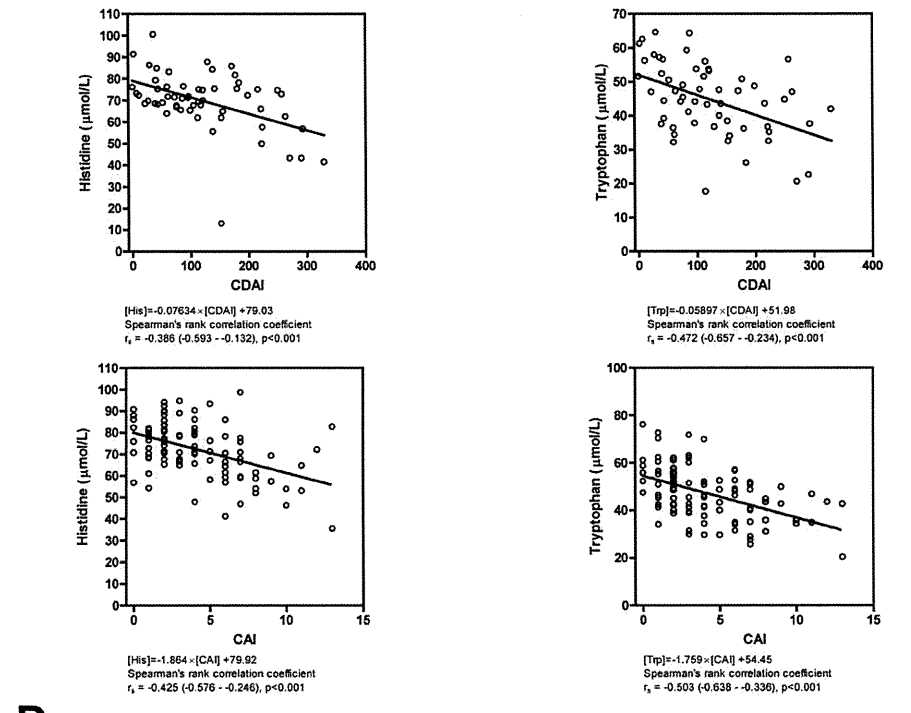
C
Histidine (µmol/L)
CDAI
[His]=-0.07634×[CDAI] +79.03
Spearman's rank correlation coefficient
r_s = -0.386 (-0.593 - -0.132), p<0.001
Tryptophan (µmol/L)
CDAI
[Trp]=-0.05897×[CDAI] +51.98
Spearman's rank correlation coefficient
r_s = -0.472 (-0.657 - -0.234), p<0.001
Histidine (µmol/L)
CAI
[His]=-1.864×[CAI] +79.92
Spearman's rank correlation coefficient
r_s = -0.425 (-0.576 - -0.246), p<0.001
Tryptophan (µmol/L)
CAI
[Trp]=-1.759×[CAI] +54.45
Spearman's rank correlation coefficient
r_s = -0.503 (-0.638 - -0.336), p<0.001

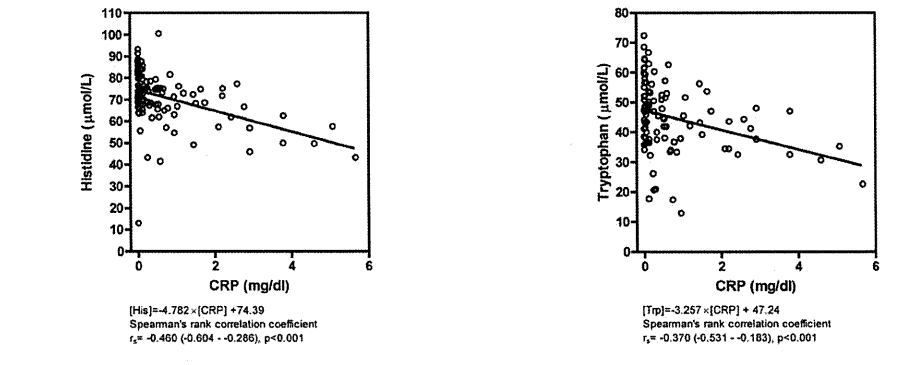
D
Histidine (µmol/L)
CRP (mg/dl)
[His]=-4.782×[CRP] +74.39
Spearman's rank correlation coefficient
r_s= -0.460 (-0.604 - -0.286), p<0.001
Tryptophan (µmol/L)
CRP (mg/dl)
[Trp]=-3.257×[CRP] + 47.24
Spearman's rank correlation coefficient
r_s= -0.370 (-0.531 - -0.183), p<0.001

Figure 1. Plasma His and Trp concentrations in IBD patients. (**A**) Plasma His concentrations are significantly lower in CD (grey bars) and UC (striped bars) patients than in HCs (white bars). Plasma Trp concentrations are significantly lower in CD patients than in HCs. The two-tailed p-values are based on the Mann-Whitney U test with the Bonferroni correction. (**B**) Plasma His and Trp concentrations are significantly lower in patients with active disease (CDa, dark grey bars, and UCa, dark striped bars) than in patients in remission (CDr, light grey bars, and UCr, light striped bars), respectively. The two-tailed p-values are based on the Mann-Whitney U test. (**C**) Significant inverse correlations between plasma His and Trp concentrations and disease activities (CDAI for CD and CAI for UC). (**D**) Significant inverse correlations between plasma His and Trp concentrations and serum CRP concentrations in CD patients. The relationships in panels C and D are shown along with their Spearman's rank correlation coefficients (r_s). Error bars show standard deviations.
doi:10.1371/journal.pone.0031131.g001

MIAI for monitoring IBD patients

Among the biggest expectations for clinical markers are their ability to objectively monitor disease activity, their use in clinical management issues, such as when to start induction therapy and how long to continue maintenance therapy, and their ability to predict prognosis, including the risk of surgery. Regarding these issues, we continuously monitored Index (CDa/CDr) and Index (UCa/UCr) to prospectively assess disease activity in several CDa and UCa patients. As shown in Figure 4, the MIAIs were reduced by induction therapy and correlated with clinical activity. These data suggest that the MIAI may have potential as a clinical marker that can monitor disease activity in individual patients for continued observation.

Discussion

In the present study, we have established the potential of the MIAI for clinical use based on our analyses of the plasma concentrations of 22 AAs and their metabolites in IBD patients.

Table 3. Spearman's rank correlation coefficients (r_s) for plasma amino acid concentrations.

	CRP			
	CD (102)		UC (95)	
	r_s	p	r_s	p
Histidine	−0.46	<0.0001	−0.29	0.0041
Tryptophan	−0.37	0.0001	−0.27	0.0093
Valine	−0.08	NS	−0.06	NS
Leucine	0.02	NS	−0.02	NS
Isoleucine	−0.07	NS	−0.02	NS
Methionine	−0.25	0.0112	−0.08	NS
Phenylalanine	0.01	NS	0.05	NS
Threonine	−0.08	NS	−0.34	0.0007
Lysine	−0.17	NS	−0.01	NS
Tyrosine	0.11	NS	−0.08	NS
Serine	−0.03	NS	−0.17	NS
Asparagine	−0.24	0.0161	−0.25	0.0163
Glutamic Acid	0.29	0.0028	0.15	NS
Glutamine	−0.13	NS	−0.13	NS
Proline	−0.04	NS	−0.19	NS
Glycine	−0.07	NS	−0.22	0.0353
Alanine	−0.21	0.0327	−0.14	NS
Cystine	0.06	NS	0.05	NS
Arginine	−0.01	NS	−0.13	NS
Ornithine	0.11	NS	0.04	NS
Citrulline	−0.11	NS	−0.08	NS
Taurine	0.08	NS	−0.15	NS

NS, not significant.
doi:10.1371/journal.pone.0031131.t003

Initially, we compared plasma aminograms of IBD patients with those of HCs and observed several differences, which may reflect nutritional condition, inflammation, and disease specific pathogenesis. In particular, the aminograms indicated that plasma His and Trp were significantly decreased in IBD patients with active disease. Furthermore, plasma His and Trp concentrations showed inverse correlations with disease activity indexes and serum CRP levels. These observations suggest that the decreased plasma His and Trp in IBD patients may reflect the chronic inflammatory condition, and that supplementation with His and Trp may be a novel therapeutic strategy for IBD. Trp is metabolized into kynurenine by the catabolic enzyme, indoleamine 2,3-dioxygenase (IDO), and Trp metabolism has recently been highlighted as an immunological regulator [13,14,15]. It is also reported that plasma kynurenine concentrations and IDO transcription levels are altered in inflamed tissue of IBD patients [16,17].

Consistent with our observations, plasma His concentrations are decreased in several chronic inflammatory disorders such as rheumatoid arthritis and chronic kidney disease [18,19], and are inversely correlated with the erythrocyte segmentation ratio (ESR) in rheumatoid arthritis patients [18]. In a clinical trial of rheumatoid arthritis patients, supplementation of 4.5 g L-His for 30 days showed clinical benefits in patients with more active and prolonged disease [20]. In chronic kidney disease, plasma His concentrations are inversely correlated with CRP and hepatocyte growth factor, markers that reflect inflammation [19]. Furthermore, enteral nutrition therapy using an elemental diet, with a His density more than twice that of the recommended WHO/FAO/UN requirement, has shown efficacy in CD [21]. Importantly, we previously reported that orally administered His ameliorates intestinal inflammation in an IL-10-deficient transfer mouse colitis model by inhibiting the production of pro-inflammatory cytokines by activated macrophages through intracellular mechanisms [22].

Plasma AA profiles are affected by the levels of protein and AA intake. Although the effects of the final meal on fasting concentrations of plasma AA are minimal, animal studies have shown that chronic alteration of protein intake affects fasting concentrations [10]. Therefore, the observed aminogram changes in IBD patients in the present study could be partially attributed to changes in dietary intake. Indeed, it has been reported that up to 85% of patients hospitalized with exacerbations of IBD have protein-energy malnutrition [23].

To date, several clinical markers that could aid the diagnosis of IBD and monitor disease activity have been reported. These include serological markers such as anti-neutrophil cytoplasmic antibodies (ANCAs) for UC and anti-*Saccharomyces cerevisiae* antibodies (ASCAs) for CD [24,25,26], although their practicality for clinical use remains controversial because of their inconvenience. Moreover, they do not reflect disease activity, so have limited use in monitoring the clinical course and therapeutic efficacy. Alternative candidate clinical markers capable of detecting inflammation and monitoring disease activity are fecal markers and serum CRP.

Fecal markers such as calprotectin have been shown to discriminate between active and inactive IBD, as well as non-

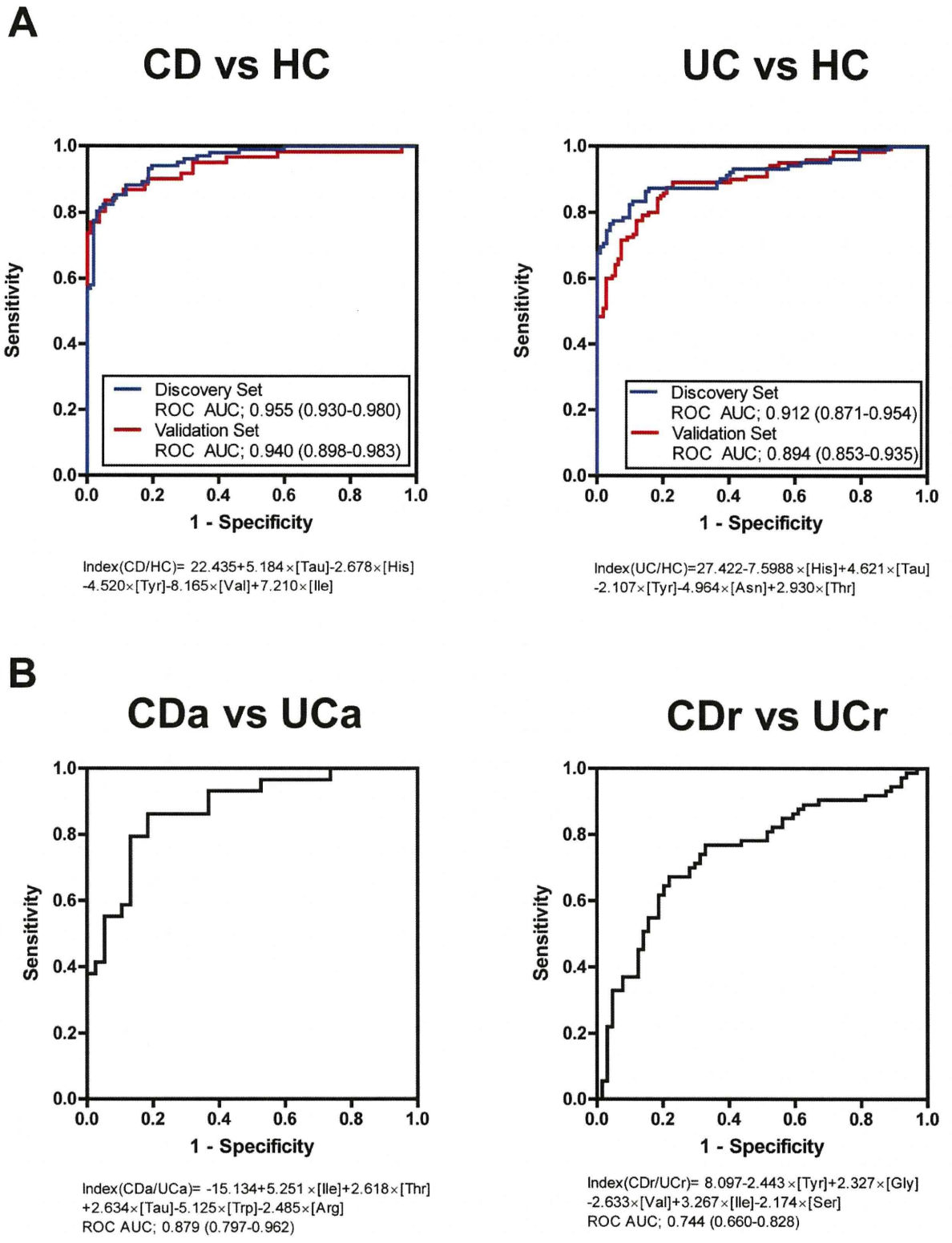

Figure 2. MIAI for clinical diagnosis of IBD. (**A**) ROCs of the MIAI for discriminating CD patients from HCs (Index (CD/HC) = 22.435+5.184×[Tau]−2.678×[His]−4.520×[Tyr]−8.165×[Val]+7.210×[Ile]) and UC patients from HCs (Index (UC/HC) = 27.422−7.5988×[His]+4.621×[Tau]−2.107×[Tyr]−4.964×[Asn]+2.930×[Thr]). (**B**) ROCs of the MIAI for discriminating CD and UC patients in discovery set (Index (CDa/UCa) = −15.134+5.251×[Ile]+2.618×[Thr]+2.634×[Tau]−5.125×[Trp]−2.485×[Arg], ROC AUC = 0.879; Index (CDr/UCr) = 8.097−2.443×[Tyr]+2.327×[Gly]−2.633×[Val]+3.267×[Ile]−2.174×[Ser], ROC AUC = 0.744). CDa, active CD; CDr, remission CD; UCa, active UC; UCr, remission UC.
doi:10.1371/journal.pone.0031131.g002

A

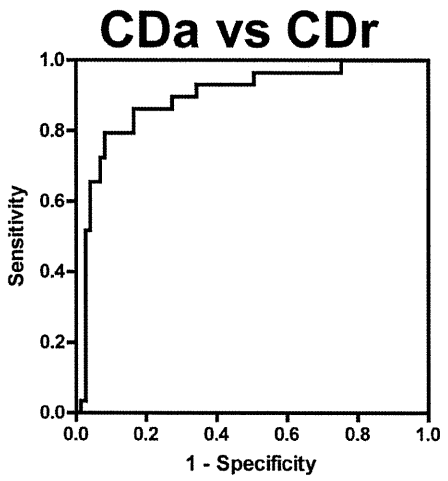

Index(CDa/CDr)=16 .474-3.342×[His]-5.190×[Trp]
+1.857×[Tau]+2.715×[Met]
ROC AUC; 0.894 (0.853-0.935)

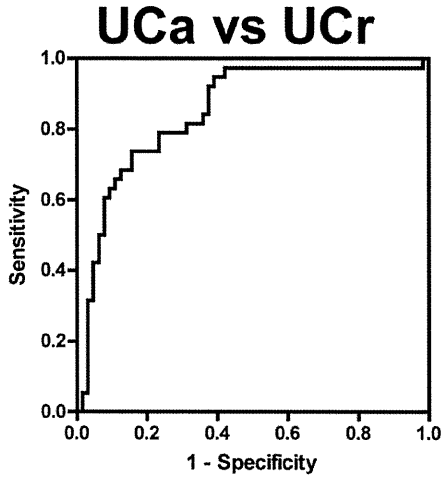

Index(UCa/UCr)=34 .019-2.926×[Trp]-1.864×[Tyr]
-4.777×[Val]-2.856×[Met]+4.604×[Ile]
ROC AUC; 0.849 (0.770-0.928)

B

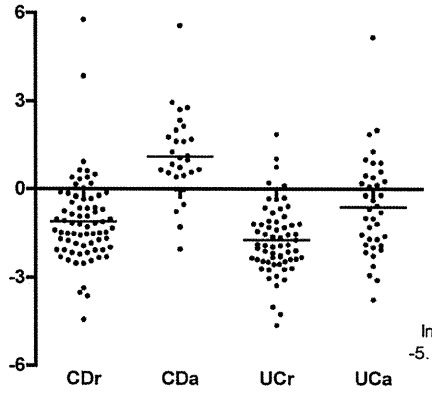

Index(CDa/CDr)=16 .474-3.342×[His]
-5.190×[Trp]+1.857×[Tau]+2.715×[Met]

C

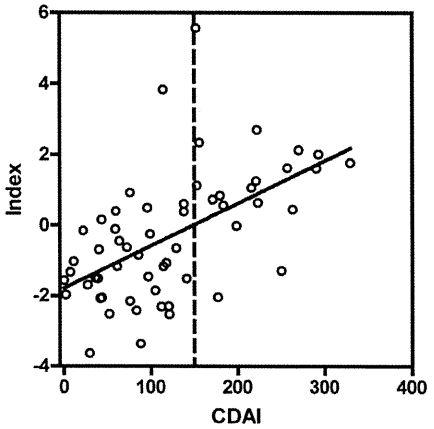

Index(CDa/CDr)=16 .474-3.342×[His]
-5.190×[Trp]+1.857×[Tau]+2.715×[Met]
Spearman's rank correlation coefficient
r_s = 0.592 (0.385-0.742, p<0 .001)
Index=0.01205×[CDAI]-1.790

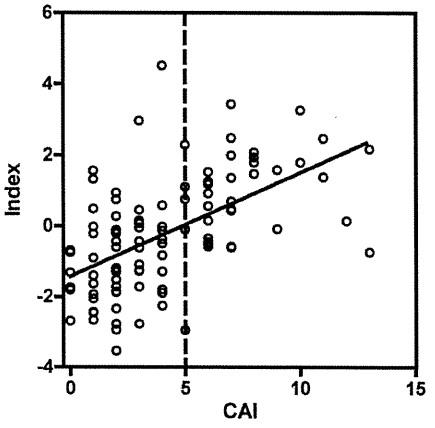

Index(UCa/UCr)=34 .019-2.926×[Trp]-1.864×[Tyr]
-4.777×[Val]-2.856×[Met]+4.604×[Ile]
Spearman's rank correlation coefficient
r_s = 0.598 (0.452-0.713, p<0 .001)
Index=0.2939×[CAI]-1.433

Figure 3. MIAI for assessing IBD disease activity. (**A**) ROCs of the MIAI for discriminating CD and UC patients with active disease and those in remission (Index (CDa/CDr) = 16.474−3.342×[His]−5.190×[Trp]+1.857×[Tau]+2.715×[Met], ROC AUC = 0.894; Index (UCa/UCr) = 34.019−2.926×[Trp]−1.864×[Tyr]−4.777×[Val]−2.856×[Met]+4.604×[Ile], ROC AUC = 0.849). (**B**) Index (CDa/CDr) cannot discriminate between active disease and remission in UC patients. (**C**) Correlations between the MIAI and disease activity indexes. Index (CDa/CDr) is correlated with the CDAI (Index = 0.01205×[CDAI]−1.790, $r_s = 0.592$, $p<0.001$) and Index (UCa/UCr) is correlated with the CAI (Index = 0.2939×[CAI]−1.433, $r_s = 0.598$, $p<0.001$).
doi:10.1371/journal.pone.0031131.g003

IBD, based on intestinal inflammation [27]. However, although fecal markers may have a high sensitivity, their disease specificity is uncertain. Serum CRP is another non-invasive biomarker used to detect inflammation and monitor disease activity, especially in CD [27,28], but its diagnostic accuracy remains controversial. By contrast, the MIAI is a convenient, non-invasive marker that may reflect disease activity more sensitively and specifically than other reported markers. Although the cost of plasma AA profiling in practical use is relatively more expensive than that of fecal calprotectin or serum CRP at present, we believe that it is possible to reduce the cost for testing plasma AA profiles by targeting several promising AAs and developing a novel enzymatic detection system of each AA as has been already achieved measurement of a BCAAs/tyrosine ratio (BTR). Since the MIAI integrates disease-specific alterations of AA metabolism, it can reflect individual conditions more objectively than analyses by solo factors (such as His). Although further investigations including prospective observations are required, the MIAI appears to be a promising marker that enables us to predict disease prognosis and manage patients accordingly.

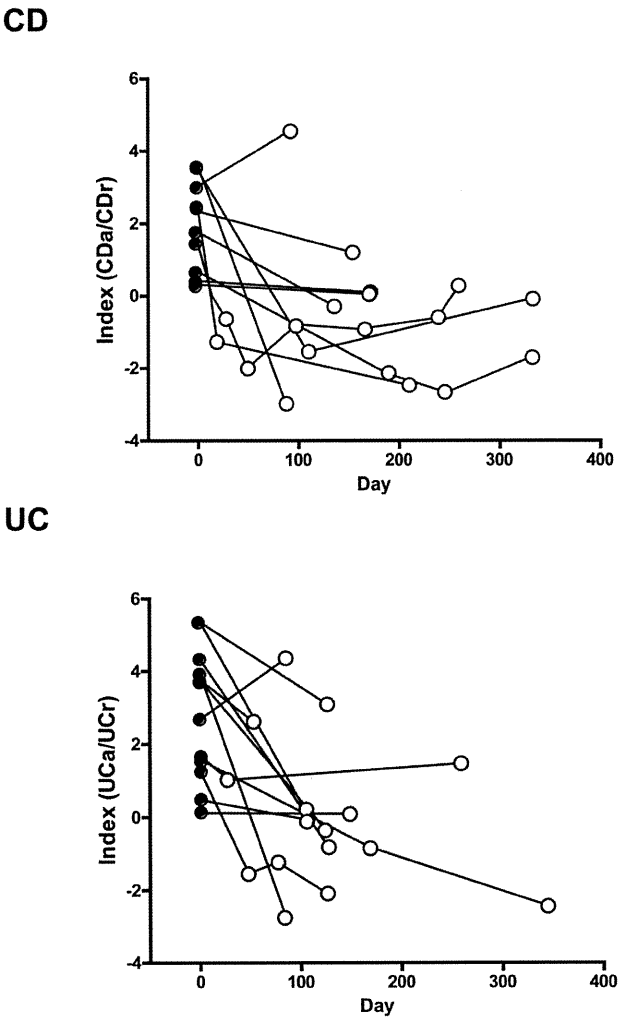

Figure 4. MIAI for monitoring IBD patients. Monitoring of some individual patients was performed prospectively. Upper panel shows the alterations in Index (CDa/CDr) in ten patients with active CD (CDAI≥150; closed circles). Remission was defined as CDAI<150 (open circles). Lower panel shows the alterations in Index (UCa/UCr) in 12 patients with active UC (CAI≥5; closed circles). Remission was defined as CAI<5 (open circles).
doi:10.1371/journal.pone.0031131.g004

In conclusion, the MIAI based on statistical modeling of plasma aminograms is a novel, non-invasive, objective parameter for the diagnosis and assessment of disease activity in IBD patients. It was shown to be capable of significantly discriminating between HCs and CD or UC patients with very high sensitivity and specificity, as well as between CD and UC patients, and those with active disease or undergoing remission. The introduction of metabolomics into IBD clinics has provided us with new insights and will contribute to the establishment of clinical parameters and our understanding of IBD pathophysiology.

Supporting Information

Figure S1 Scatter plots of plasma AA concentrations in individual HCs and IBD patients. Each panel represents the scatterplot of two plasma AAs from individual HCs (green), CD patients (red), and UC patients (blue). Panel shows correlation plots of the concentrations of 22 AAs.
(TIF)

Figure S2 A general imbalance of branched-chain AAs (BCAAs) in IBD patients. (**A**) Correlation plots of leucine (Leu), valine (Val), and isoleucine (Ile). Ellipses show that 95% of the values are in a bivariate normal distribution. (**B**) Mean plasma Leu, Ile, and Val concentrations in active CD (CDa), remission CD (CDr), active UC (UCa), and remission UC (UCr) patients. Error bars show standard deviations. The two-tailed p-values are based on the Mann-Whitney U test.
(TIF)

Table S1 Candidates of MIAI for clinical diagnosis of IBD.
(DOC)

Methods S1 Statistical analysis.
(DOC)

Acknowledgments

The authors thank Makoto Naganuma, Nobuhiko Kamada, Taku Kobayashi, Motoko Izumiya, Hitoshi Ichikawa, Riko Ichikawa, Yasunari Takada, Tetsuro Takayama, Tomohisa Sujino, Kazuaki Yoneno, Yohei Mikami, and Jun Miyoshi (Keio University) for technical assistance and discussion.

Author Contributions

Conceived and designed the experiments: T.Hisamatsu AA RS NO MS. Performed the experiments: T.Hisamatsu MH AA RS NO TA MS. Analyzed the data: MH TM AA MU. Contributed reagents/materials/

analysis tools: SO MK KM TY NI TK HO YI MY. Wrote the paper: T.Hisamatsu. Proofread and approved the manuscript: T.Hisamatsu SO MH TM AA MU MK KM TY NI TK HO YI MY RS NO TA MS T.Hibi.

References

1. Hibi T, Ogata H (2006) Novel pathophysiological concepts of inflammatory bowel disease. J Gastroenterol 41: 10–16.
2. Xavier RJ, Podolsky DK (2007) Unravelling the pathogenesis of inflammatory bowel disease. Nature 448: 427–434.
3. Felig P (1975) Amino acid metabolism in man. Annu Rev Biochem 44: 933–955.
4. Brosnan JT (2003) Interorgan amino acid transport and its regulation. J Nutr 133: 2068S–2072S.
5. Shiota T, Nakatsukasa H, Fujiwara M, Takei N, Yamauchi Y, et al. (1984) Plasma amino acid imbalance in alcoholic liver cirrhosis. Biochem Med 32: 181–188.
6. Holm E, Sedlaczek O, Grips E (1999) Amino acid metabolism in liver disease. Curr Opin Clin Nutr Metab Care 2: 47–53.
7. Ferenci P, Wewalka F (1978) Plasma amino acids in hepatic encephalopathy. J Neural Transm Suppl: 87–94.
8. Soeters PB, Fischer JE (1976) Insulin, glucagon, aminoacid imbalance, and hepatic encephalopathy. Lancet 2: 880–882.
9. Maeda J, Higashiyama M, Imaizumi A, Nakayama T, Yamamoto H, et al. (2010) Possibility of multivariate function composed of plasma amino acid profiles as a novel screening index for non-small cell lung cancer: a case control study. BMC Cancer 10: 690.
10. Noguchi Y, Zhang QW, Sugimoto T, Furuhata Y, Sakai R, et al. (2006) Network analysis of plasma and tissue amino acids and the generation of an amino index for potential diagnostic use. Am J Clin Nutr 83: 513S–519S.
11. Winship DH, Summers RW, Singleton JW, Best WR, Becktel JM, et al. (1979) National Cooperative Crohn's Disease Study: study design and conduct of the study. Gastroenterology 77: 829–842.
12. Lichtiger S, Present DH, Kornbluth A, Gelernt I, Bauer J, et al. (1994) Cyclosporine in severe ulcerative colitis refractory to steroid therapy. N Engl J Med 330: 1841–1845.
13. Puccetti P, Grohmann U (2007) IDO and regulatory T cells: a role for reverse signalling and non-canonical NF-kappaB activation. Nat Rev Immunol 7: 817–823.
14. Munn DH, Zhou M, Attwood JT, Bondarev I, Conway SJ, et al. (1998) Prevention of allogeneic fetal rejection by tryptophan catabolism. Science 281: 1191–1193.
15. Romani L, Fallarino F, De Luca A, Montagnoli C, D'Angelo C, et al. (2008) Defective tryptophan catabolism underlies inflammation in mouse chronic granulomatous disease. Nature 451: 211–215.
16. Forrest CM, Gould SR, Darlington LG, Stone TW (2003) Levels of purine, kynurenine and lipid peroxidation products in patients with inflammatory bowel disease. Adv Exp Med Biol 527: 395–400.
17. Wolf AM, Wolf D, Rumpold H, Moschen AR, Kaser A, et al. (2004) Overexpression of indoleamine 2,3-dioxygenase in human inflammatory bowel disease. Clin Immunol 113: 47–55.
18. Gerber DA (1975) Low free serum histidine concentration in rheumatoid arthritis. A measure of disease activity. J Clin Invest 55: 1164–1173.
19. Watanabe M, Suliman ME, Qureshi AR, Garcia-Lopez E, Barany P, et al. (2008) Consequences of low plasma histidine in chronic kidney disease patients: associations with inflammation, oxidative stress, and mortality. Am J Clin Nutr 87: 1860–1866.
20. Pinals RS, Harris ED, Burnett JB, Gerber DA (1977) Treatment of rheumatoid arthritis with L-histidine: a randomized, placebo-controlled, double-blind trial. J Rheumatol 4: 414–419.
21. Akobeng AK, Thomas AG (2007) Enteral nutrition for maintenance of remission in Crohn's disease. Cochrane Database Syst Rev: CD005984.
22. Andou A, Hisamatsu T, Okamoto S, Chinen H, Kamada N, et al. (2009) Dietary histidine ameliorates murine colitis by inhibition of proinflammatory cytokine production from macrophages. Gastroenterology 136: 564–574 e562.
23. Wall AJ, Kirsner JB (1975) Ulcerative colitis and Crohn's disease of the colon: Symptoms, signs, and laboratory aspects. In: Kirsner JB, Shorter RG, eds. Inflammatory Bowel Disease Lea & Febiger, Philadelphia. pp 101–108.
24. Vernier G, Sendid B, Poulain D, Colombel JF (2004) Relevance of serologic studies in inflammatory bowel disease. Curr Gastroenterol Rep 6: 482–487.
25. Targan SR, Landers CJ, Yang H, Lodes MJ, Cong Y, et al. (2005) Antibodies to CBir1 flagellin define a unique response that is associated independently with complicated Crohn's disease. Gastroenterology 128: 2020–2028.
26. Dotan I, Fishman S, Dgani Y, Schwartz M, Karban A, et al. (2006) Antibodies against laminaribioside and chitobioside are novel serologic markers in Crohn's disease. Gastroenterology 131: 366–378.
27. Langhorst J, Elsenbruch S, Koelzer J, Rueffer A, Michalsen A, et al. (2008) Noninvasive markers in the assessment of intestinal inflammation in inflammatory bowel diseases: performance of fecal lactoferrin, calprotectin, and PMN-elastase, CRP, and clinical indices. Am J Gastroenterol 103: 162–169.
28. Vermeire S, Van Assche G, Rutgeerts P (2004) C-reactive protein as a marker for inflammatory bowel disease. Inflamm Bowel Dis 10: 661–665.

TECHNICAL REPORTS

nature medicine

Functional engraftment of colon epithelium expanded *in vitro* from a single adult Lgr5$^+$ stem cell

Shiro Yui[1,6], Tetsuya Nakamura[2,6], Toshiro Sato[3,5], Yasuhiro Nemoto[1], Tomohiro Mizutani[1], Xiu Zheng[1], Shizuko Ichinose[4], Takashi Nagaishi[1], Ryuichi Okamoto[2], Kiichiro Tsuchiya[1], Hans Clevers[3] & Mamoru Watanabe[1]

Adult stem-cell therapy holds promise for the treatment of gastrointestinal diseases. Here we describe methods for long-term expansion of colonic stem cells positive for leucine-rich repeat containing G protein-coupled receptor 5 (Lgr5$^+$ cells) in culture. To test the transplantability of these cells, we reintroduced cultured GFP$^+$ colon organoids into superficially damaged mouse colon. The transplanted donor cells readily integrated into the mouse colon, covering the area that lacked epithelium as a result of the introduced damage in recipient mice. At 4 weeks after transplantation, the donor-derived cells constituted a single-layered epithelium, which formed self-renewing crypts that were functionally and histologically normal. Moreover, we observed long-term (>6 months) engraftment with transplantation of organoids derived from a single Lgr5$^+$ colon stem cell after extensive *in vitro* expansion. These data show the feasibility of colon stem-cell therapy based on the *in vitro* expansion of a single adult colonic stem cell.

Epithelial stem cells maintain tissue homeostasis throughout the gastrointestinal tract[1–3]. The Wnt, bone morphogenetic protein (BMP) and Notch cascades function together to regulate stem-cell maintenance[4,5]. *Lgr5* marks stem cells in small intestinal and colonic crypts[6] and in gastric units[7]. *Bmi1* may mark distinct stem cells in the proximal small intestine[8]. It has been shown that freshly isolated intestinal epithelium can be transplanted in rodents after resident epithelium has been surgically removed[9,10]. We previously developed a three-dimensional culture technique that allows expansion of single Lgr5$^+$ stem cells from small intestine[11], stomach[7] and colon[12]. The resulting organoids then expand and self organize into an epithelial architecture that is reminiscent of that seen in *in vivo* histology. Moreover, the growing organoids maintain their tissue identity even after prolonged culture. Here we sought to evaluate whether the cultured Lgr5$^+$ cells faithfully represent the tissue-resident Lgr5$^+$ stem cells and, thus, are able to regenerate epithelial tissue *in vivo*. Considering that the colon is very vulnerable to disease in humans, we focused on colonic stem cells in our analyses.

RESULTS

Long-term, serum-free culture system for colonic organoids

We subjected the colons of adult mice to a combination of enzymes[13], reducing agents[14] and mechanical disruption. The resulting crypt fragments were mostly devoid of α smooth muscle actin gene (*Acta2*)-expression–positive non-epithelial components and consisted of a mix of cadherin 1, type 1, E-cadherin (*Cdh1*)$^+$ cells expressing terminal differentiation marker genes (*Muc2*, *CA2* and *ChgA*) and Lgr5$^+$ stem cells (**Supplementary Fig. 1a,b**).

The addition of R-spondin 1 (Rspo1), Noggin and epidermal growth factor (EGF), which are all essential to small intestine culture[11], did not maintain the growth of colonic crypts. We therefore developed the following 'TMDU (Tokyo Medical and Dental University) protocol': we embedded crypts in type I collagen in serum-free medium with Wnt3a, hepatocyte growth factor (HGF)[15,16] and BSA, in addition to Rspo1, Noggin and EGF (**Supplementary Fig. 1c**). Sequential imaging of the cultures revealed rapid growth of cystic structures (**Fig. 1a**). Wnt3a, Rspo1 and BSA were essential to this growth (**Supplementary Fig. 1d**). As predicted by previous results[17,18], Rspo1 could be substituted with Wnt3a (data not shown). Although Noggin, EGF and HGF were not essential for growth of the colonic crypts, each enhanced their growth (**Supplementary Fig. 1e**). The colonic organoids rarely had buds (**Fig. 1a**, **Supplementary Fig. 2a** and **Supplementary Video 1**). Of note, small intestinal organoids also generate cystic structures when Wnt3a is added to them[19].

The colonic organoids were single layered (**Supplementary Fig. 2b**), and all the cells within were positive for Cdh1 expression (**Fig. 1b**). The basal membranes of the organoids faced outward (**Fig. 1b**). Ki67$^+$ cells were present in the colonic organoids (**Fig. 1b**), as were alcian blue–positive goblet cells, chromogranin A (ChgA)$^+$ enteroendocrine cells, carbonic anhydrase II (CA2)$^+$ colonocytes and cytochrome c oxidase subunit I (COX1)$^+$ tuft cells[20] (**Fig. 1b**). Transmission electron microscopy revealed epithelial characteristics such as microvilli (**Fig. 1c**) and junctional complexes (**Fig. 1d**) in the organoids. However, stromal cells were absent (**Supplementary Fig. 2c**). Mitotic cells with condensed chromosomes were present in the organoids (**Fig. 1e**), and goblet cells (**Fig. 1f**) and enteroendocrine cells (**Fig. 1g**) could also be clearly detected.

[1]Department of Gastroenterology and Hepatology, Graduate School, Tokyo Medical and Dental University, Bunkyo-ku, Tokyo, Japan. [2]Department of Advanced Therapeutics for Gastrointestinal Diseases, Tokyo Medical and Dental University, Bunkyo-ku, Tokyo, Japan. [3]Hubrecht Institute and University Medical Centre, Utrecht, The Netherlands. [4]Research Center for Medical and Dental Sciences, Tokyo Medical and Dental University, Bunkyo-ku, Tokyo, Japan. [5]Present address: Department of Gastroenterology, Keio University School of Medicine, Shinjuku-ku, Tokyo, Japan. [6]These authors contributed equally to this work. Correspondence should be addressed to H.C. (h.clevers@hubrecht.eu) or M.W. (mamoru.gast@tmd.ac.jp).

Received 30 July 2011; accepted 29 November 2011; published online 11 March 2012; doi:10.1038/nm.2695

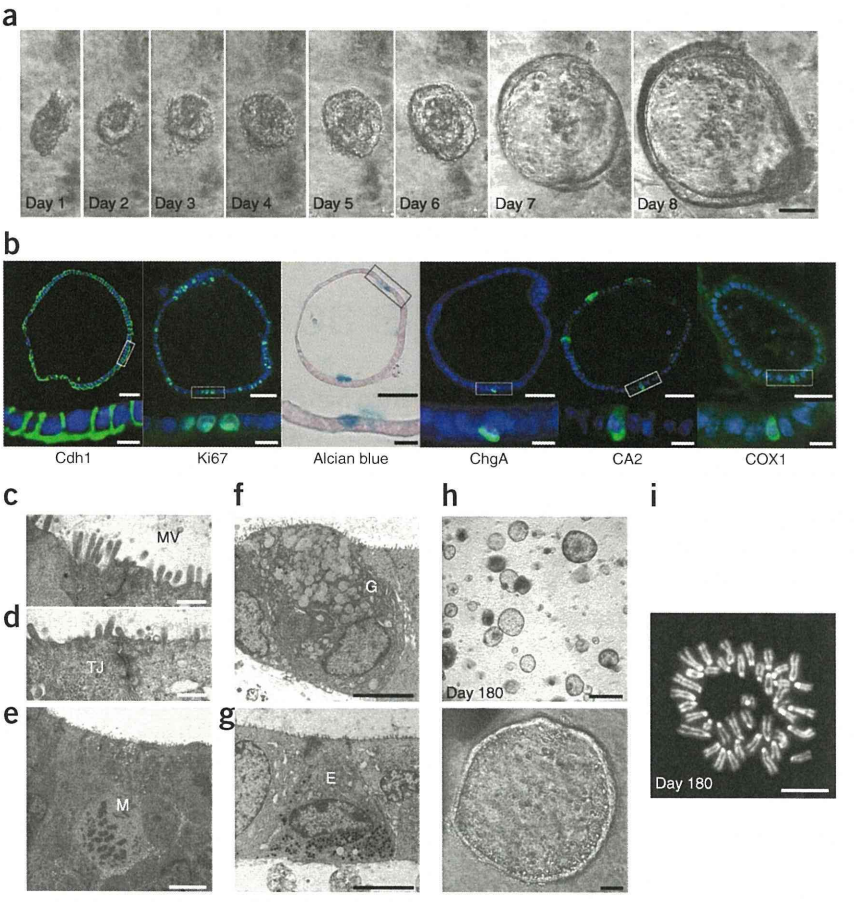

Figure 1 Long-term, serum-free culture of colonic epithelial cells. (**a**) A representative colonic crypt growing as a cystic structure. Scale bar, 50 μm. Time-lapse images of another colonic crypt are shown in **Supplementary Figure 2a** and **Supplementary Video 1**. (**b**) Histology of the colonic organoids at day 8 of culture. Cdh1$^+$ cells, actively proliferating Ki67$^+$ cells (green) and terminally differentiated cells stained with alcian blue (blue, goblet cells) or immunostained with ChgA (green, enteroendocrine cells), CA2 (green, colonocytes) or COX1 (green, tuft cells) are shown. Higher magnification views of the boxed areas are shown at the bottom. DAPI staining was performed, except for the experiments in which we performed alcian blue staining. Scale bars, top, 50 μm; bottom, 10 μm. (**c**–**g**) Transmission electron microscopy analysis for organoids at day 8. (**c**,**d**) Microvilli (MV) and intracellular tight junctions (TJ) are shown. (**e**) Mitotic (M) cells showing chromatin condensation. (**f**,**g**) Goblet cells (G) with mucus granules (**f**) and enteroendocrine cells (E) with electron dense granules (**g**) are shown. Scale bars: **c**,**d**, 0.5 μm; **e**–**g**, 5 μm. Low-power views of **f** and **g** are also shown in **Supplementary Figure 2c**. (**h**) The culture at day 180 (top) and its representative organoid (bottom). Scale bars, top, 500 μm; bottom, 50 μm. Images of the growth of a single cell after passage are shown in **Supplementary Figure 3** and **Supplementary Video 2**. (**i**) Metaphase spread of a cell at day 180 shows a normal karyotype ($2n = 40$). Scale bar, 10 μm.

The organoids could be passaged weekly at a 1:2 ratio (**Supplementary Fig. 3** and **Supplementary Video 2**). Addition of the Rho kinase inhibitor Y-27632 (ref. 21) improved the replating efficiency of the organoids[11]. We successfully propagated organoids for more than 6 months without clear alterations of morphology (**Fig. 1h**) or karyotype (**Fig. 1i**).

Lgr5$^+$ cells are enriched in colonic organoids

We tracked the expression of *Lgr5* over 60 d and found a substantial elevation during the first 8 d of observation (**Fig. 2a**). We found no change in the expression of *ChgA* and *CA2*, whereas *Muc2* expression was repressed in the first 8 d (**Fig. 2a**). Addition of a combination of Wnt3a, Rspo1 and BSA induced *Lgr5* expression (**Fig. 2b**). *Lgr5* expression was further upregulated by the addition of Noggin, which is an antagonist of BMP[22] (**Fig. 2b**). The Notch pathway suppresses the

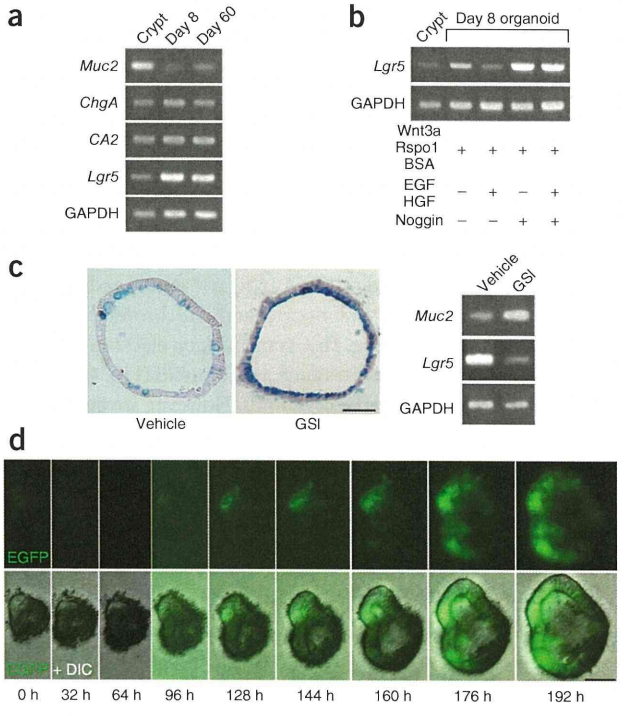

Figure 2 Lgr5$^+$ stem cells are enriched in cultured organoids. (**a**) RT-PCR analysis of the colonic crypts immediately after isolation (crypt) or organoids cultured for 8 or 60 d. *Lgr5* was upregulated and stayed constant thereafter. Differentiation marker genes (*Muc2*, *ChgA* and *CA2*) were expressed over 60 d. The primers used are listed in **Supplementary Table 1**. (**b**) RT-PCR shows that *Lgr5* upregulation is mediated by a combination of minimum factors (Wnt3a, Rspo1 and BSA) and Noggin but not by EGF and HGF. (**c**) Notch signal-mediated cell fate determination *in vitro*. Cultured organoids were treated with GSI, LY-411575 or vehicle alone from day 4 to day 8. Organoids stained with alcian blue are shown (left). Scale bar, 50 μm. RT-PCR shows that the expression of *Muc2* is upregulated, whereas the expression of *Lgr5* is reciprocally downregulated in organoids treated with LY-411575 (GSI, right). Similar results were obtained in three independent experiments, and representative data are shown. (**d**) A time-lapse imaging of a growing colonic crypt obtained from an *Lgr5-EGFP-ires-CreERT2* mouse over 192 h. The top panel shows EGFP and the bottom panel shows merged images of EGFP and differential interference contrast (DIC). Scale bar, 50 μm. The corresponding video (**Supplementary Video 3**) and similar results from another example are available as **Supplementary Figure 4a** and **Supplementary Video 4**.

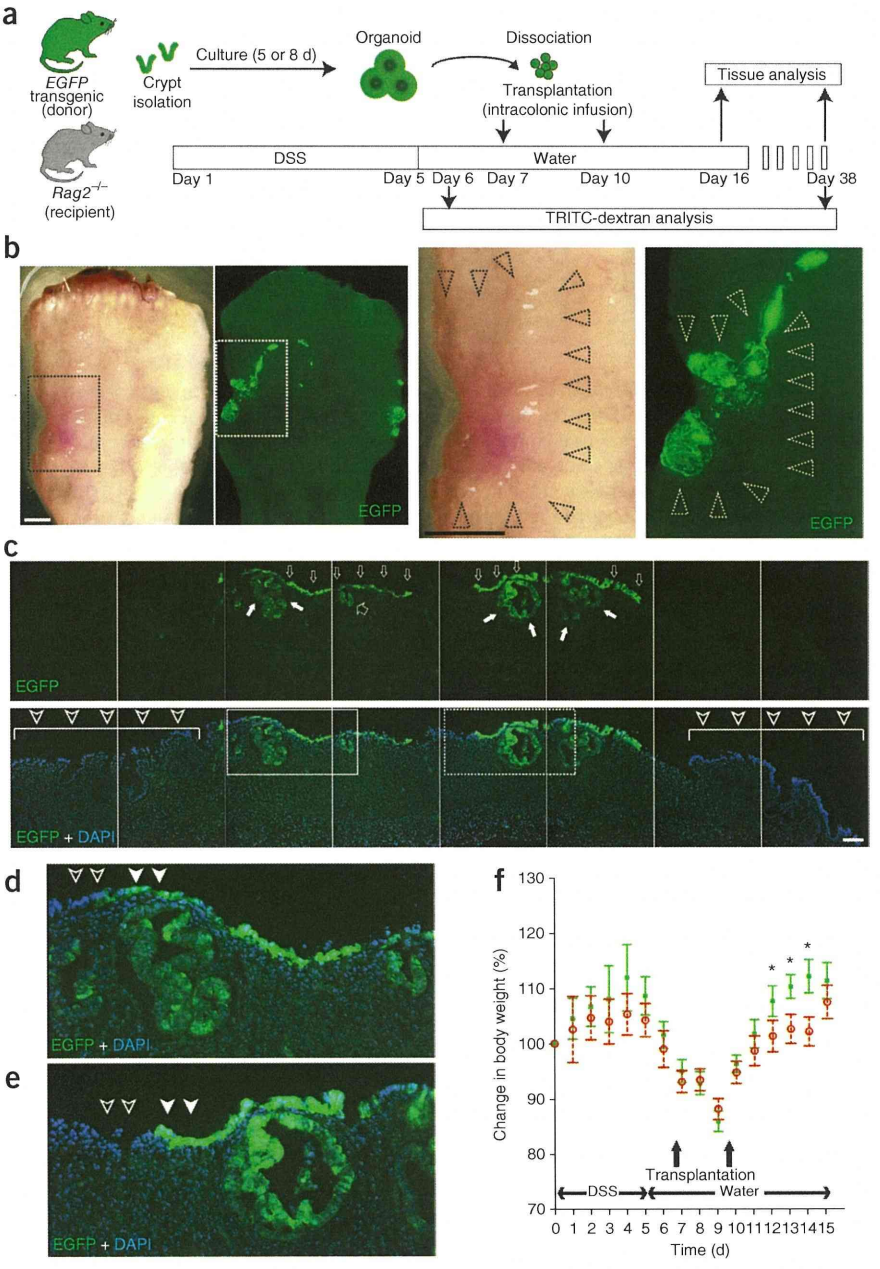

Figure 3 Transplantation of cultured cells improves acute colitis. (**a**) Experimental protocols. (**b**) Recipient colon at 6 d after transplantation. Low-power views (stereoscopic and fluorescent images) are shown on the left. High-power views of the areas in the dotted squares are shown in the right. The black dotted arrowheads show a depressed area surrounded by edematous mucosa. EGFP$^+$ areas overlapping the damaged region (white dotted arrowheads) are also shown. Note that the outline of the tissue is not precisely the same in the stereoscopic and fluorescent images, as they were acquired on different microscopes. Scale bars, 1 mm. (**c**) Histology of the EGFP$^+$ area shown in **b**. EGFP (top) and the merged image with DAPI staining (bottom). EGFP$^+$ cells cover the damaged mucosa that intervene separate areas preserving crypt structures (bottom, arrowheads). EGFP$^+$ cells constitute flat linings (top, narrow open arrow) or an invagination (top, wide open arrows), the latter of which is reminiscent of crypts. EGFP$^+$ cystic structures were also observed in the EGFP$^+$ cells (top, filled white arrows). The regions in the solid- and dotted-line boxes are shown at higher magnification in **d** and **e**, respectively. Scale bar, 100 μm. (**d**) High-power view of the solid box in **c**. (**e**) High-power view of the dotted box in **c**. (**f**) *Rag2*$^{-/-}$ mice were given DSS for 5 d, and then transplantation ($n = 6$) or sham-transplantion ($n = 6$) was performed. On day 16, the presence of engraftment was retrospectively assessed after the mice were killed. The body weights of the mice with EGFP$^+$ engraftment (green squares, $n = 4$) and sham-transplanted controls (red open circles, $n = 6$) are presented as a percentage of their initial weight. Error bars, s.e.m. $^*P < 0.05$ (Student's t test).

differentiation of progenitors[23,24] and stem cells[25] toward secretory lineages. We treated the colonic organoids with LY-411575, a γ-secretase inhibitor (GSI) that is capable of inhibiting Notch signaling[26,27]. Notch inhibition induced a goblet-cell phenotype with an increased level of *Muc2* mRNA and a reciprocal decrease in the expression of *Lgr5* (**Fig. 2c**).

We next performed live imaging of colonic organoids obtained from *Lgr5-EGFP-internal ribosome entry site (ires)-CreERT2* mice[6] in which an enhanced GFP (EGFP) and tamoxifen-inducible Cre recombinase cassette is integrated into the *Lgr5* locus. The *Lgr5*-promoter–driven EGFP expression initially stayed at a marginal level but then increased beginning at day 5 (**Fig. 2d**, **Supplementary Fig. 4a** and **Supplementary Videos 3** and **4**). We confirmed the expansion of Lgr5$^+$ cells at a single-cell resolution (**Supplementary Fig. 4b**). Over multiple passages, the *Lgr5-EGFP* locus tended to become silenced, whereas the wild-type *Lgr5* allele remained active (**Fig. 2a,b**). Taken together, colonic Lgr5$^+$ stem cells were able to self renew and expand *in vitro*.

Cultured colonic organoids rescue damaged epithelium

We next tested the transplantability of the cultured organoids (**Fig. 3a**). We induced colonic mucosal damage by providing immunocompromised *Rag2*$^{-/-}$ mice with colitis-inducing dextran sulfate sodium (DSS)[28] for 5 d. Most of the mice developed acute colitis characterized by weight loss, bloody stool, diarrhea and epithelial injury in the distal colon. At 7 and 10 d after initiating DSS administration, we dissociated the organoids cultured from *EGFP* transgenic mice[29] into small fragments, suspended them in a Matrigel-containing PBS and instilled them by enema in recipient mice.

At 16 d after the start of DSS administration, the recipient colons showed varying degrees of recovery. Multiple EGFP$^+$ areas appeared as well-demarcated patches in the treated colons (**Fig. 3b**). We did not observe any EGFP$^+$ areas in colons not treated with DSS (data not shown). Histologically, the EGFP$^+$ cells covered the submucosa and were located between the less damaged recipient tissues (**Fig. 3c**). The EGFP$^+$ cells formed flat or slightly invaginated linings (**Fig. 3c**). We also observed large cystic EGFP$^+$ structures below the surface of the treated colons (**Fig. 3c**). Some of the EGFP$^+$ areas connected to the recipients' epithelium (**Fig. 3d**), whereas others repopulated areas that were devoid of recipient epithelium (**Fig. 3e**). Notably, the body weights of the mice with engraftment were

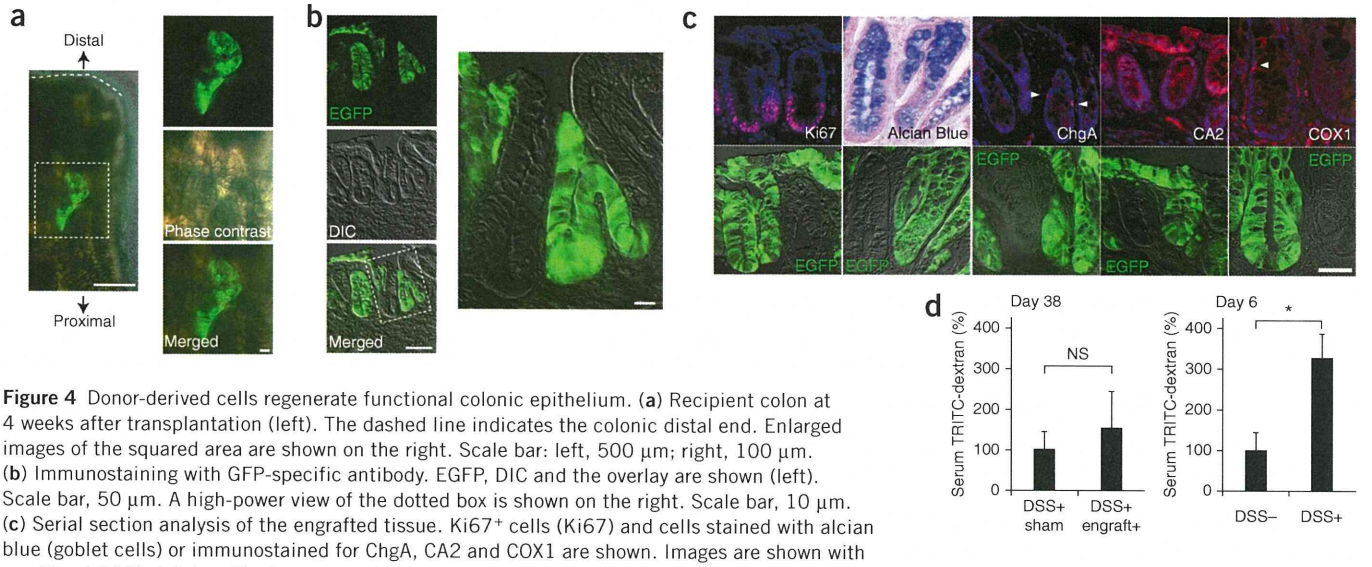

Figure 4 Donor-derived cells regenerate functional colonic epithelium. (**a**) Recipient colon at 4 weeks after transplantation (left). The dashed line indicates the colonic distal end. Enlarged images of the squared area are shown on the right. Scale bar: left, 500 μm; right, 100 μm. (**b**) Immunostaining with GFP-specific antibody. EGFP, DIC and the overlay are shown (left). Scale bar, 50 μm. A high-power view of the dotted box is shown on the right. Scale bar, 10 μm. (**c**) Serial section analysis of the engrafted tissue. Ki67$^+$ cells (Ki67) and cells stained with alcian blue (goblet cells) or immunostained for ChgA, CA2 and COX1 are shown. Images are shown with or without DAPI staining. The bottom row shows neighboring sections stained for GFP. Arrowheads point to ChgA$^+$ or COX1$^+$ cells. Scale bar, 50 μm. (**d**) After DSS colitis induction, transplantation ($n = 6$) or sham transplantation ($n = 6$) was performed. Mice were administered TRITC-dextran by gavage before killing on day 38. Four out of six colons in the transplanted group had EGFP$^+$ engraftment, and the serum TRITC concentration in these mice is shown (DSS+ engraft+; $n = 4$) as a percentage of that in the sham-transplanted group (DSS+ sham; $n = 6$). As a control, DSS colitis was induced (DSS+; $n = 6$) or uninduced (DSS–; $n = 6$) in *Rag2*$^{-/-}$ mice, and these mice were subjected for the same assay on day 6 without transplantation. Data are shown as a percentage of the concentrations in uninduced mice. Error bars, s.e.m. $^*P < 0.05$, NS, not significant (Student's *t* test).

higher than those of sham-transplanted mice (**Fig. 3f**; with statistically significant results at days 12, 13 and 14, $P < 0.05$).

At 4 weeks after transplantation, tube-like EGFP$^+$ crypts appeared in the distal colon (**Fig. 4a**) that were morphologically indistinguishable from the surrounding EGFP$^-$ epithelium (**Fig. 4b**). Notably, the engrafted crypts were entirely EGFP$^+$, indicating the presence of EGFP$^+$ stem cells (**Fig. 4b**). Cells in the lower part of the EGFP$^+$ crypts were normally Ki67$^+$, and the EGFP$^+$ crypts contained all

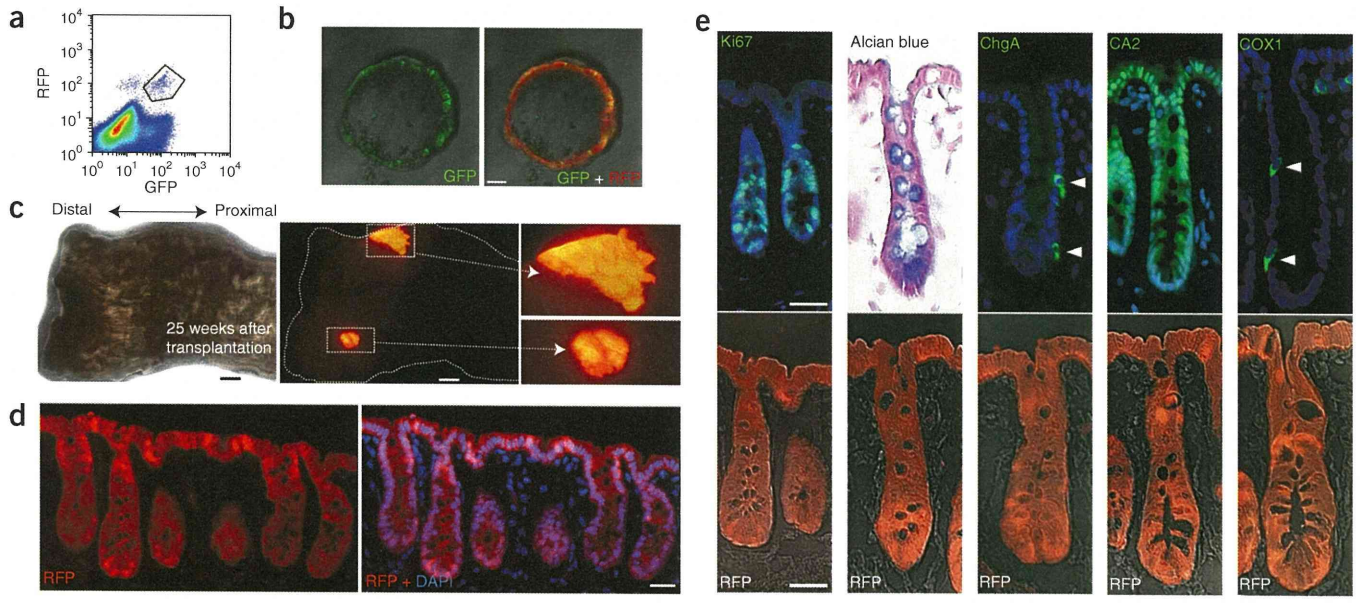

Figure 5 Single Lgr5$^+$ stem-cell–derived cultured cells serve as long-lived, multipotential stem cells *in vivo*. (**a**) Fluorescence-activated cell sorting analysis of colonic cells of *R26R-Confetti* mice crossed with *Lgr5-EGFP-ires-CreERT2* mice 3 d after Cre induction. The EGFP$^+$ and RFP$^+$ populations located in the box were sorted and cultured. (**b**) Images are shown of one out of four organoids grown from sorted single Lgr5$^+$ cells at day 6. EGFP$^+$ stem cells are scattered in the organoid (left), with all the offspring being positive for RFP (right). Scale bar, 50 μm. (**c**) Images of the recipient colon at 25 weeks after transplantation. The phase-contrast view of the recipient colon is shown on the left. The fluorescent image shows the tissue contains RFP$^+$ grafts (right). Scale bar, 1 mm. Enlarged images of the boxed areas are also shown (2.7-fold magnification). (**d**) Immunostaining of the RFP$^+$ engraft at 25 weeks after transplantation. An image of RFP-specific antibody staining (left) and an image of RFP staining merged with DAPI staining (right) are shown. Scale bar, 50 μm. (**e**) Serial section analysis of the engrafted RFP$^+$ tissue at 25 weeks after transplantation. The top panels show Ki67, alcian blue, ChgA, CA2 or COX1 staining with or without nuclei stained by DAPI. The bottom panels show the adjacent sections stained for RFP. Arrowheads point to ChgA$^+$ enteroendocrine cells and COX1$^+$ tuft cells. Scale bars, 50 μm.

terminally differentiated cell types (**Fig. 4c**). We probed the epithelial permeability of the engrafts using tetramethylrhodamine isothiocyanate (TRITC)-conjugated dextran (TRITC-dextran). Blood TRITC concentrations in transplanted mice were comparable to those in control mice, indicating a maintenance of epithelial barrier function in these engrafts (**Fig. 4d**). Notably, transplantation was less successful with freshly isolated donor cells ($P < 0.05$, Mann-Whitney U test; **Supplementary Fig. 5**), suggesting that the expansion of stem cells during the culture is associated with a higher success rate of transplantation. In addition, Matrigel-containing organoid suspensions transplanted better than organoids suspended in PBS (**Supplementary Fig. 5**; $P < 0.05$, Mann-Whitney U test), proposing a role for the simultaneous supply of extracellular matrix in successful transplantation.

Engraftment of organoids derived from a single Lgr5$^+$ cell

We next sought to initiate the protocol described above from a single stem cell (**Supplementary Fig. 6a**). We crossed *Lgr5-EGFP-ires-CreERT2* mice with *R26R-Confetti* reporter mice[30]. In the resulting offspring, tamoxifen-induced Cre activation resulted in Cre-mediated recombination at the *Rosa26* locus in individual Lgr5$^+$ stem cells, leading to stochastically selected expression of one out of four fluorescent proteins: red fluorescent protein (RFP), cyan fluorescent protein (CFP), GFP or yellow fluorescent protein (YFP). At 3 d after Cre activation, we sorted cells double positive for Lgr5-EGFP and Confetti-RFP, which consisted of ~0.02% of the total cells (**Fig. 5a**), equivalent to ~100 cells per mouse.

We cultured the sorted cells after a limiting dilution (100 cells per 96 well) using the Hubrecht protocol (Online Methods; protocol described previously[12] with addition of Y-27632 in the first 2 d). Four stem cells double positive for Lgr5-EGFP and Confetti-RFP grew out, which was comparable to the culture efficiency of small intestinal stem cells[11] (**Fig. 5b**). Organoids were expanded to more than 100 wells in >10 weeks, frozen and shipped. After thawing, we recovered the cells under the TMDU protocol. We transplanted ~500 organoids per recipient mouse, as described above. Analyses at 4, 17, 21 and 25 weeks after transplantation revealed the presence of grafts in these mice (**Fig. 5c** and **Supplementary Figs. 6b,c** and **7a**). At 25 weeks after transplantation, RFP$^+$ cells still generated a single-layered epithelium. We noted no sign of adenomatous or dysplastic change in any of the transplanted areas (**Fig. 5d**). Again, all differentiated cell types, as well as Ki67$^+$ proliferating cells, were present at normal ratios (**Fig. 5e** and **Supplementary Fig. 7b**).

DISCUSSION

Here we describe methodologies to isolate, culture and transplant Lgr5$^+$ colon stem cells. Our observations confirm that *Lgr5* marks genuine stem cells that retain their self-renewal and multilineage-differentiation properties even after prolonged culture. A major difference between small-intestinal and colon-culture conditions is in the latter's requirement for Wnt. Although Wnt factors can initiate Wnt signals on their own, R-spondins (such as Rspo1) can only augment preexisting Wnt signals[31]. Because Paneth cells produce Wnt3, they serve as the center of organization of the stem cell niche[19]. At the colon crypt bottoms, secretory cells are located between the Lgr5$^+$ stem cells that—like Paneth cells—express CD24 (ref. 19). However, these CD24$^+$ secretory cells do not produce a sufficient amount of Wnt proteins *in vitro* (data not shown). Therefore, colon organoids cannot grow from Rspo1 alone but, rather, also require exogenous Wnt.

This study provides proof of principle that cultured Lgr5$^+$ cells can be used for stem-cell therapy to repair damaged epithelium. Transplanted cells adhere to and cover superficially damaged tissue. Further, engrafted recipient mice had higher body weights than ungrafted controls, implying a beneficial role for the donor cells in DSS-induced acute colitis. Although further optimization is clearly needed, the current study implies that *in vitro* expansion and transplantation of gastrointestinal stem cells may be a promising option for patients with severe gastrointestinal epithelial injuries.

Lgr5$^+$ stem cells divide once every day *in vivo*[6], thus defying the Hayflick limit[32]. They appear similarly unrestricted in their proliferative capacity *in vitro*, while they retain their original tissue identity. It is of interest that the Lgr5 protein is now known to reside in the Wnt receptor complex to function as a receptor for Rspo1 (refs. 33,34), which is a crucial component of long-term organoid culture systems that we have developed. As the resulting organoids have now been proven to be transplantable, the Lgr5$^+$ stem cell isolation and expansion technology may provide a simple and safe avenue for the development of new regenerative and gene-therapy strategies.

METHODS

Methods and any associated references are available in the online version of the paper at http://www.nature.com/naturemedicine/.

Note: Supplementary information is available on the Nature Medicine website.

ACKNOWLEDGMENTS

We thank M. Okabe (Osaka University) for EGFP transgenic mice and Y. Kato, J. Inazawa, I. Sekiya (TMDU), H. Snippert and R. Vries (Hubrecht Institute) for technical assistance. This study was supported by Grant-in-Aid for Scientific Research from the Japanese Ministry of Education, Culture, Sports, Science and Technology, by the Health and Labour Sciences Research Grants for Research on Intractable Diseases from Ministry of Health, Labour and Welfare of Japan, and by a grant from the European Research Council and from the Dutch Cancer Foundation.

AUTHOR CONTRIBUTIONS

T. Nakamura, H.C. and M.W. designed the study. S.Y., T. Nakamura and T.S. performed experiments and analyzed data. T. Nakamura, T.S. and H.C. wrote the paper. Y.N., T. Nagaishi and K.T. assisted in transplantation experiments. T.M., X.Z. and K.T. gave support in gene analysis. R.O. helped with the immunohistochemistry. S.I. advised on the electron microscopy. H.C. and M.W. gave conceptual advice and supervised the project.

COMPETING FINANCIAL INTERESTS

The authors declare competing financial interests: details accompany the full-text HTML version of the paper at http://www.nature.com/naturemedicine/.

Published online at http://www.nature.com/naturemedicine/.
Reprints and permissions information is available online at http://www.nature.com/reprints/index.html.

1. Potten, C.S., Booth, C. & Pritchard, D.M. The intestinal epithelial stem cell: the mucosal governor. *Int. J. Exp. Pathol.* **78**, 219–243 (1997).
2. Bjerknes, M. & Cheng, H. Intestinal epithelial stem cells and progenitors. *Methods Enzymol.* **419**, 337–383 (2006).
3. Barker, N., van de Wetering, M. & Clevers, H. The intestinal stem cell. *Genes Dev.* **22**, 1856–1864 (2008).
4. Crosnier, C., Stamataki, D. & Lewis, J. Organizing cell renewal in the intestine: stem cells, signals and combinatorial control. *Nat. Rev. Genet.* **7**, 349–359 (2006).
5. Radtke, F. & Clevers, H. Self-renewal and cancer of the gut: two sides of a coin. *Science* **307**, 1904–1909 (2005).
6. Barker, N. *et al.* Identification of stem cells in small intestine and colon by marker gene *Lgr5*. *Nature* **449**, 1003–1007 (2007).
7. Barker, N. *et al.* Lgr5^{+ve} stem cells drive self-renewal in the stomach and build long-lived gastric units *in vitro*. *Cell Stem Cell* **6**, 25–36 (2010).
8. Sangiorgi, E. & Capecchi, M.R. *Bmi1* is expressed *in vivo* in intestinal stem cells. *Nat. Genet.* **40**, 915–920 (2008).
9. Avansino, J.R., Chen, D.C., Woolman, J.D., Hoagland, V.D. & Stelzner, M. Engraftment of mucosal stem cells into murine jejunum is dependent on optimal dose of cells. *J. Surg. Res.* **132**, 74–79 (2006).
10. Tait, I.S., Evans, G.S., Flint, N. & Campbell, F.C. Colonic mucosal replacement by syngeneic small intestinal stem cell transplantation. *Am. J. Surg.* **167**, 67–72 (1994).

11. Sato, T. *et al.* Single Lgr5 stem cells build crypt-villus structures *in vitro* without a mesenchymal niche. *Nature* **459**, 262–265 (2009).
12. Sato, T. *et al.* Long-term expansion of epithelial organoids from human colon, adenoma, adenocarcinoma, and Barrett's epithelium. *Gastroenterology* **141**, 1762–1772 (2011).
13. Booth, C., Patel, S., Bennion, G.R. & Potten, C.S. The isolation and culture of adult mouse colonic epithelium. *Epithelial Cell Biol.* **4**, 76–86 (1995).
14. Whitehead, R.H., Demmler, K., Rockman, S.P. & Watson, N.K. Clonogenic growth of epithelial cells from normal colonic mucosa from both mice and humans. *Gastroenterology* **117**, 858–865 (1999).
15. Kanayama, M. *et al.* Hepatocyte growth factor promotes colonic epithelial regeneration via Akt signaling. *Am. J. Physiol. Gastrointest. Liver Physiol.* **293**, G230–G239 (2007).
16. Tahara, Y. *et al.* Hepatocyte growth factor facilitates colonic mucosal repair in experimental ulcerative colitis in rats. *J. Pharmacol. Exp. Ther.* **307**, 146–151 (2003).
17. Kim, K.A. *et al.* Mitogenic influence of human R-spondin1 on the intestinal epithelium. *Science* **309**, 1256–1259 (2005).
18. Wei, Q. *et al.* R-spondin1 is a high affinity ligand for LRP6 and induces LRP6 phosphorylation and β-catenin signaling. *J. Biol. Chem.* **282**, 15903–15911 (2007).
19. Sato, T. *et al.* Paneth cells constitute the niche for Lgr5 stem cells in intestinal crypts. *Nature* **469**, 415–418 (2011).
20. Gerbe, F. *et al.* Distinct ATOH1 and Neurog3 requirements define tuft cells as a new secretory cell type in the intestinal epithelium. *J. Cell Biol.* **192**, 767–780 (2011).
21. Watanabe, K. *et al.* A ROCK inhibitor permits survival of dissociated human embryonic stem cells. *Nat. Biotechnol.* **25**, 681–686 (2007).
22. Haramis, A.P. *et al. De novo* crypt formation and juvenile polyposis on BMP inhibition in mouse intestine. *Science* **303**, 1684–1686 (2004).
23. Fre, S. *et al.* Notch signals control the fate of immature progenitor cells in the intestine. *Nature* **435**, 964–968 (2005).
24. van Es, J.H. *et al.* Notch/γ-secretase inhibition turns proliferative cells in intestinal crypts and adenomas into goblet cells. *Nature* **435**, 959–963 (2005).
25. van Es, J.H., de Geest, N., van de Born, M., Clevers, H. & Hassan, B.A. Intestinal stem cells lacking the Math1 tumour suppressor are refractory to Notch inhibitors. *Nat. Commun.* **1**, 18 (2010).
26. Wong, G.T. *et al.* Chronic treatment with the γ-secretase inhibitor LY-411,575 inhibits β-amyloid peptide production and alters lymphopoiesis and intestinal cell differentiation. *J. Biol. Chem.* **279**, 12876–12882 (2004).
27. Okamoto, R. *et al.* Requirement of Notch activation during regeneration of the intestinal epithelia. *Am. J. Physiol. Gastrointest. Liver Physiol.* **296**, G23–G35 (2009).
28. Wirtz, S., Neufert, C., Weigmann, B. & Neurath, M.F. Chemically induced mouse models of intestinal inflammation. *Nat. Protoc.* **2**, 541–546 (2007).
29. Okabe, M., Ikawa, M., Kominami, K., Nakanishi, T. & Nishimune, Y. 'Green mice' as a source of ubiquitous green cells. *FEBS Lett.* **407**, 313–319 (1997).
30. Snippert, H.J. *et al.* Intestinal crypt homeostasis results from neutral competition between symmetrically dividing Lgr5 stem cells. *Cell* **143**, 134–144 (2010).
31. Binnerts, M.E. *et al.* R-Spondin1 regulates Wnt signaling by inhibiting internalization of LRP6. *Proc. Natl. Acad. Sci. USA* **104**, 14700–14705 (2007).
32. Hayflick, L. & Moorhead, P.S. The serial cultivation of human diploid cell strains. *Exp. Cell Res.* **25**, 585–621 (1961).
33. de Lau, W. *et al.* Lgr5 homologues associate with Wnt receptors and mediate R-spondin signalling. *Nature* **476**, 293–297 (2011).
34. Carmon, K.S., Gong, X., Lin, Q., Thomas, A. & Liu, Q. R-spondins function as ligands of the orphan receptors LGR4 and LGR5 to regulate Wnt/β-catenin signaling. *Proc. Natl. Acad. Sci. USA* **108**, 11452–11457 (2011).

ONLINE METHODS

Mice. *Rag2*$^{-/-}$ mice were from Taconic Farms and Central Laboratories for Experimental Animals. *EGFP* transgenic mice[29], *Lgr5-EGFP-ires-CreERT2* mice[6] and *R26R-Confetti* mice[30] are described elsewhere. Male and female mice were randomly used for all experiments. All animal experiments were performed with the approval of the Institutional Animal Care and Use Committee of TMDU.

TMDU protocol for crypt isolation and three-dimensional culture. The colonic tissue was minced and digested. The crypts were further purified by mechanical disruption and density gradient centrifugation. A total of 2,000 crypts were suspended in 200 µl of the collagen type I solution (Nitta Gelatin Inc.) and placed in 48-well plates. After polymerization, 500 µl of Advanced DMEM/F12 containing BSA (Sigma), mouse EGF (mEGF) (PeproTech), mWnt3a, mRspo1, mHGF and mNoggin (all from R&D Systems) was added (TMDU medium). For passage, the gel was digested, and then the organoids were disaggregated with EDTA. The dissociated organoids were mixed in type I collagen solution and used for culture. A Rho kinase inhibitor, Y-27632, was added for the first 2 d after the cells were propagated. Where indicated, to induce goblet cell differentiation, organoids were treated with LY-411575, a GSI. See details in the **Supplementary Methods**.

Chromosome analysis. Chromosome karyotyping was performed according to a standard protocol as detailed in the **Supplementary Methods**.

Stereomicroscopy, phase-contrast imaging and histology. Images were acquired on either a fluorescence microscope equipped with phase-contrast setting (BZ-8000, KEYENCE), a fluorescent stereomicroscope system MVX10 (Olympus) or a fluorescence microscope DeltaVision system (Applied Precision). For histology and immunohistochemistry, tissues and organoids were fixed, sequentially dehydrated in sucrose in PBS, and frozen in OCT compound (Tissue Tek). Cryosections were examined by conventional H&E, alcian blue staining and a spectrum of immunohistochemical reactions, as detailed in the **Supplementary Methods**.

Transmission electron microscopy. Transmission electron microscopy was performed in a standard fashion and is detailed in the **Supplementary Methods**.

Live imaging. Live imaging was performed on the DeltaVision system. A culture dish placed on the microscope stage was covered with a chamber in which a humidified premixed gas consisting of 5% CO_2 and 95% air was infused, and the whole setup was set at 37 °C. DIC and fluorescent images were acquired at 20-min intervals. The data were processed using Softworx (Applied Precision) and, if necessary, image editing was performed using Adobe Photoshop Elements 7.0.

Semi-quantitative RT-PCR. Semi-quantitative RT-PCR was performed in standard fashion. The primer sequences used are listed in **Supplementary Table 1**. PCR products were separated on agarose gels and visualized using ImageQuant TL system (GE Healthcare).

Sorting and Hubrecht-protocol culture for single Lgr5$^+$ cells. Tamoxifen was injected into *R26R-Confetti* mice crossed with *Lgr5-EGFP-ires-CreERT2* mice, and the colonic crypts from the resulting mice were isolated 3 d later. Epithelial cells were dissociated with TrypLE express (Invitrogen) and analyzed by MoFlo (DakoCytomation). Viable single cells were gated, and then the cells doubly positive for EGFP and RFP were sorted and embedded in Matrigel (BD Bioscience) on 96-well plates. An Advanced DMEM/F12 culture medium supplemented with penicillin and streptomycin, 4-(2-hydroxyethyl)-1-piperazineethanesulfonic acid (HEPES), glutamax, N2, B27 (all from Invitrogen) and growth factors (EGF, noggin and R-spondin) was diluted 1:1 with Wnt3a-conditioned medium and used as Hubrecht medium. Y-27632 was included for the first 2 d to avoid anoikis. Growth factors were added every other day, and the entire medium was changed every 4 d. See the **Supplementary Methods** for additional details.

Transplantation experiments. For the EGFP$^+$ cell transplantations, cells isolated from colon tissues were cultured for 5 or 8 d according to the TMDU protocol and used as donor cells. For single Lgr5$^+$-cell–derived organoid transplantation, cells were expanded based on the Hubrecht protocol and then cryopreserved. The cells were then shipped, thawed and further cultured. Acute colitis was induced by feeding 6-week-old *Rag2*$^{-/-}$ mice with 3.0% DSS (molecular weight 10,000; Ensuiko Sugar Refining Co.) dissolved in drinking water for 5 d (days 1–5). At 7 and 10 d after the start of DSS administration, donor cells equivalent to those from ~500 organoids were instilled into colonic lumen as a suspension. After infusion, the anal verge was glued for 6 h. After the transplantation on day 10, mice were maintained as usual before they were killed and analyzed. See the **Supplementary Methods** for additional details.

TRITC-dextran permeability assay. Intestinal permeability was assessed by enteral administration of TRITC-dextran (molecular mass 4.4 kDa; Sigma). Transplanted or sham-transplanted mice were gavaged with TRITC-dextran 4 h before killing on day 38. Whole blood was obtained at the time of killing, and then the colonic tissues were examined for whether the EGFP$^+$ engrafts were present. TRITC-dextran measurements were performed on an ARVO MX (PerkinElmer), with serial dilutions of TRITC-dextran used as a standard curve.

Statistical analyses. Data are shown as means ± s.e.m. Data for **Figures 3f**, **4d** and **Supplementary Figure 7b** were statistically analyzed by the two-sample Student's *t* test. The data for **Supplementary Figure 5** showed non-normal distributions and were analyzed by Mann-Whitney *U* test. Statistical significance for comparisons was assigned at $P < 0.05$.

Additional methods. Detailed methodology is described in the **Supplementary Methods**.

Meta-analysis of Published Studies Identified Eight Additional Common Susceptibility Loci for Crohn's Disease and Ulcerative Colitis

Junji Umeno, MD,[*†] Kouichi Asano, MD,*[*†‡] Tomonaga Matsushita, MD,*[*†] Takayuki Matsumoto, MD,*[†] Yutaka Kiyohara, MD,*[‡] Mitsuo Iida, MD,*[†] Yusuke Nakamura, MD,*[§] Naoyuki Kamatani, MD,*[‖] and Michiaki Kubo, MD*[*†‡]

Background: Both ulcerative colitis (UC) and Crohn's disease (CD) have a complex etiology involving multiple genetic and environmental factors. Many genome-wide association studies (GWAS) and subsequent replication studies revealed that both diseases share some of the susceptibility loci; however, common genetic factors for both diseases are not fully elucidated. This study is aimed to identify the common genetic factors for CD and UC by a meta-analysis of published studies.

Methods: We first reviewed the 10 GWAS for CD to select candidate single nucleotide polymorphisms (SNPs). Next, we performed a PubMed literature search up to June 30, 2010 and carried out a systemic review of published studies that examined the association of CD susceptibility loci in UC patients. Meta-analysis was carried out using the inverse variance-weighted method or the DerSimonian-Laird method after estimating the heterogeneity among the studies. The data for highly linked SNPs were combined. Finally, we performed a meta-analysis of 43 published studies in 45 SNPs located at 33 loci by using a total of 4852 to 31,125 subjects.

Results: We confirmed the association of 17 reported common susceptibility loci. Moreover, we found associations at eight additional loci: *GCKR, ATG16L1, CDKAL1, ZNF365, LRRK2-MUC19, C13orf31, PTPN2*, and *SBNO2*. The genetic risk of each locus was modest (odds ratios ranged from 1.05–1.22) except *IL23R*.

Conclusions: These results indicate that CD and UC share many susceptibility loci with small genetic effect. Our data provide further understanding of the common pathogenesis between CD and UC.

(Inflamm Bowel Dis 2011;000:000–000)

Key Words: single nucleotide polymorphism, meta-analysis, shared genetic risk, ulcerative colitis, Crohn's disease

Ulcerative colitis (UC) and Crohn's disease (CD), the two most common forms of inflammatory bowel disease (IBD), have a complex etiology involving multiple genetic and environmental factors. Family and twin studies have clearly indicated the involvement of genetic factors in the development of both diseases.[1] Moreover, UC and CD exist in the same family with higher frequency than the co-occurrence by chance alone, suggesting an etiological relationship between the two diseases.[2,3] Since the chronic relapsing intestinal inflammation induced by the dysregulated mucosal immune response to commensal enteric bacteria is one of the common pathogenesis of CD and UC, it is important to understand the shared genetic factors for both diseases.

Recent genome-wide association studies (GWAS) for CD[4–13] have identified more than 30 susceptibility loci and provided new insights into the immunopathogenesis of this disease, implicating an important role of genes of the innate and adaptive immune systems for disease occurrence.[14] Similarly, several GWAS for UC[15–20] have identified more than 10 susceptibility loci. A comparison of the results of these studies and additional association studies has identified 18 common susceptibility loci between CD and UC, including *IL23R, JAK2, STAT3, BSN-MST1, CCNY-CREM, KIF21B, NKX2-3, IL12B, ORMDL3, ICOSLG, LOC441108, IRGM, CCR6, TNFSF15*, 5p13, 6p21, 7p12,

Additional Supporting Information may be found in the online version of this article.

Received for publication December 6, 2010; Accepted December 17, 2010.

From the *Laboratory for Genotyping Development, Center for Genomic Medicine, RIKEN, Yokohama Institute, Japan, †Department of Medicine and Clinical Science, Kyushu University, Fukuoka, Japan, ‡Department of Environmental Medicine, Graduate School of Medical Sciences, Kyushu University, Fukuoka, Japan, §Laboratory of Molecular Medicine, Human Genome Center, Institute of Medical Science, University of Tokyo, Tokyo, Japan, ‖Laboratory for Statistical Analysis, Center for Genomic Medicine, RIKEN, Yokohama Institute, Japan.

Supported in part by the Ministry of Education, Culture, Sports, Science and Technology of Japan.

Reprints: Michiaki Kubo, MD, PhD, Laboratory for Genotyping Development, Center for Genomic Medicine, RIKEN Yokohama Institute, 1-7-22 Suehiro-cho, Tsurumi-ku, Yokohama, Kanagawa, 230-0045, Japan (e-mail: mkubo@src.riken.jp)

DOI 10.1002/ibd.21651

Published online in Wiley Online Library (wileyonlinelibrary.com).

and 21q21.[16,19–25] However, considering the strong heritability of both diseases, several common genetic factors may not have been found yet and meta-analysis of published studies is one approach by which these factors may be identified. Nevertheless, to our knowledge, only a handful of meta-analysis for common susceptibility loci between UC and CD have been performed, most notably for *NOD2*, *PTPN22*, *ATG16L1*, and *IRGM*.[26–31] Therefore, we performed a comprehensive meta-analysis of published studies that examined the association of CD susceptibility loci in UC patients to clarify common genetic factors for both diseases.

MATERIALS AND METHODS

Single Nucleotide Polymorphism (SNP) Selection for a Literature Search

We reviewed the literature of 10 GWAS for CD including meta-analyses[4–13] published before June 30, 2010. Initially, we selected 62 SNPs for the literature search based on the following criteria: 1) SNPs showed a significant level of overall *P*-value less than 5×10^{-7} in an initial GWAS for CD; and 2) located at non-MHC region because of the broad and strong linkage disequilibrium across the MHC region (Supporting Information Table 1).

Literature search strategy and study selection criteria

We performed a PubMed literature search (National Center for Biotechnology Information [NCBI]; http://www.ncbi.nlm.nih.gov/pubmed/) up to June 30, 2010 using the following terms: (ulcerative colitis or inflammatory bowel disease) and (polymorphism* or variant* or loci or locus). References from the selected publications were manually scanned to identify other relevant studies. Studies were included if: 1) they were case–control studies for Caucasian UC; 2) they included at least 100 UC cases; 3) they were published in English; 4) they examined the selected SNPs or the highly linked SNPs with the selected ones ($r^2 \geq 0.95$ in the HapMap Southern Utah residents of European descent [CEU] samples [release #27, build 36]); and 5) they provided enough data to calculate odds ratios (ORs) and 95% confidence intervals (CIs). For publications using overlapping samples, we discarded the smaller dataset (13 studies). The literature search and data extraction were conducted by two authors (K.A. and J.U.). Disagreement over eligibility was resolved by a detailed discussion after review by one additional author (T.M.). Details of this search strategy are shown in Figure 1. Finally, a total of 43 articles[16,19–25,27,29,30,32–63] were included in the meta-analysis (Table 1).

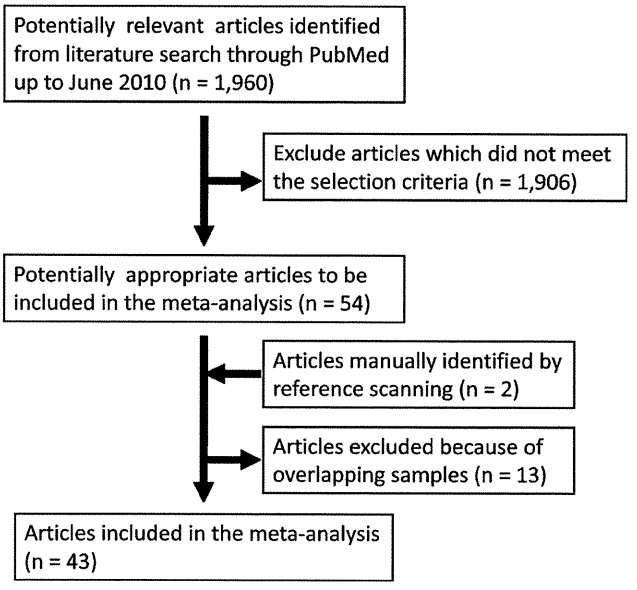

FIGURE 1. Flowchart of search strategy for meta-analysis.

Meta-analysis

We assessed heterogeneity across the studies using Cochran's *Q* test and I^2 statistics. *P*-value > 0.10 and I^2 statistics < 25% indicated a lack of heterogeneity.[64] If there was no heterogeneity among the studies, meta-analysis was carried out using the inverse variance-weighted method. This method is a fixed-effect model based on the assumption that the true OR of all studies is the same and no interstudy variance exist. When heterogeneity was present, we used the DerSimonian-Laird method. This method is a random-effect model which considers interstudy variance to estimate the combined OR. Publication bias was investigated by funnel plot and evaluated using Egger's test.[65] Funnel plot is a scatterplot which displays the OR of each study on the X axis against sample size on the Y axis. If there is no publication bias, OR will be distributed symmetrically and its variation may be smaller in larger studies. The degree of symmetry of funnel plot was estimated by Egger's test. We considered the evidence of significant publication bias as an obvious asymmetry of funnel plot and Egger's *P*-value < 0.05. All statistical analyses were undertaken using R (http://www.r-project.org/).

We basically used reported ORs and 95% CIs of the published studies to perform meta-analysis. Since 15 out of 43 articles did not report OR or 95% CI, we calculated OR and 95% CI of each SNP using genotype data in eight studies,[21,27,33,35,38,39,53,61] sample size and minor allele frequency (MAF) in three studies,[32,34,37] *P*-value and OR in three studies,[16,20,59] and *P*-value and MAF in one study.[48] Among the 62 SNPs initially selected, we excluded seven SNPs (rs10801047 [1q31], rs1002922 [5p13], rs10512734 [5p13], rs1373692 [5p13], rs3810936 [*TNFSF15*], rs7848647 [*TNFSF15*], and rs5743289 [*NOD2/CARD15*]) because these SNPs had not been studied in at least two studies. In addition, the data of SNPs in *ATG16L1* (rs2241880, rs10210302, and rs3828309), *BSN-MST1* (rs9858542 and rs3197999), 5p13 (rs4613763 and rs17234657), *IRGM* (rs13361189, rs1000113, and rs11747270), *TNFSF15*

TABLE 1. Studies Included in the Meta-analysis

	Study	Reference	Year	Population	Case	Control
1	Ogura	32	2001	USA	182	287
2	Cuthbert	33	2002	UK	566	290
3	Esters	34	2004	Belgium	173	165
4	Büning	35	2005	Hungary	128	208
5	Martín	36	2005	Spain	544	812
6	Waller	37	2006	UK	512	750
7	Oostenbrug	27	2006	Netherlands	207	276
8	Crawford	38	2007	USA	172	104
9	Cucchiara	39	2007	Italy	186	347
10	Tremelling	40	2007	UK and Scotland	975	1345
11	Büning_1	41	2007	Germany and Hungary	296	707
12	Cummings	42	2007	UK	647	1134
13	Glas	43	2007	Germany	456	1381
14	Economou	44	2007	Greece	180	100
15	Büning_2	45	2007	German and Hungary	294	845
16	Roberts	46	2007	New Zealand	466	591
17	Glas	47	2008	Germany	507	1615
18	Lappalainen	48	2008	Finnland	459	292
19	Márquez	49	2008	Spain	363	546
20	Franke	15	2008	Germany	1103	1817
21	Fisher	21	2008	UK	1740	1492
22	Lakatos	50	2008	Hungary	149	149
23	Okazaki	51	2008	Canada	117	310
24	Roberts	52	2008	New Zealand	475	576
25	Fowler	53	2008	Australia	543	1244
26	Weersma_1	54	2009	Netherlands	1120	1350
27	Anderson	23	2009	UK	2527	3028
28	Silverberg	16	2009	USA and Canada	1052	2571
29	Weersma_2	24	2009	Belgium and Netherlands	1442	1045
30	Einarsdottir	55	2009	Sweden	455	280
31	Glas	56	2009	Germany	476	1503
32	Newman	57	2009	Canada	402	1005
33	Palomino-Morales	29	2009	Spain	425	572
34	Márquez_1	30	2009	Spain	368	745
35	Márquez_2	58	2009	Spain	405	800
36	Törkvist	59	2010	Sweden	935	1460
37	Festen	25	2010	Netherlands	1455	1902
38	Sventoraityte	60	2010	Lithuania	123	186
39	Lacher	61	2010	Germany	132	253
40	Cénit	62	2010	Spain	442	1692
41	Franke	19	2010	Germany	1043	1703
42	McGovern_GWAS1	20	2010	USA	723	2880
	McGovern_GWAS2	20	2010	Sweden	948	1408
	McGovern_GWAS3	20	2010	USA and Canada	1022	2503
	McGovern_Replication1	20	2010	Italy	993	826
	McGovern_Replication2	20	2010	Netherlands	1016	754
43	Perdigones	63	2010	Spain	662	1361